Thank you very much Editor for the minor comments and recommendations. Below you will find our point-by-point response:

1) Line 41 in the abstract states that wind stress was analyzed. As this analysis was taken out at the suggestion of a reviewer, "wind stress" should be removed from this line.

R: Yes, we removed "Wind stress"

2) Lines 81-84. These lines were added at the suggestion of a reviewer. It would be helpful to readers if the authors could add what they mean by "warmer and more saline waters." Give some data on the mean salinity and temperature of the CW and how it compares with the rest of the surface water in the Gulf of Mexico.

R: We add differences for salinity and temperature as follow:

"CW enters in the GoM via the LC with specific biological (i.e., low Chl-a) and physical characteristics (warmer by ~0.6 units and less saline waters by ~0.5 units)".

3) Lines 264-275: this paragraph doesn't make sense as written. It includes the sentence (line 268) "From May to August, the monthly ratio descended to 1.36." However, in line 272 the August ratio is given as 1.60. Line 268 also says "Ratio values greater than 1 were found in February…" Presumably this should be greater than 1.6. Please check the numbers given for each month and the mean values for the seasonal periods. Is this really a biannual cycle? It looks as though numbers are low in summer, high in fall/winter/spring.

R: We agree about the confusion and we recalculated the ratios (see figure below) and improved the section as follows (lines 268-275):

Ratio values were 1.37 in January, increased to 1.45 in February, and to 1.60 in March, then peaked in April (1.63) to decrease in May (1.47) and June (1.46), reaching a low value in August (1.27). The monthly ratio then increased in September to 1.55, decreased slightly in October (153), reached a maximum value in November to 1.65, and settled to 1.55 in December. A plot of these monthly ratios clearly shows a strong biannual signal peaking in April and November (not pictured). Chang and Oey (2012, 2013) proposed that the LC intrusion and the shedding of the LCE followed a biannual cycle. This biannual cycle can also be related to the annual lowest and highest values of the ratio.

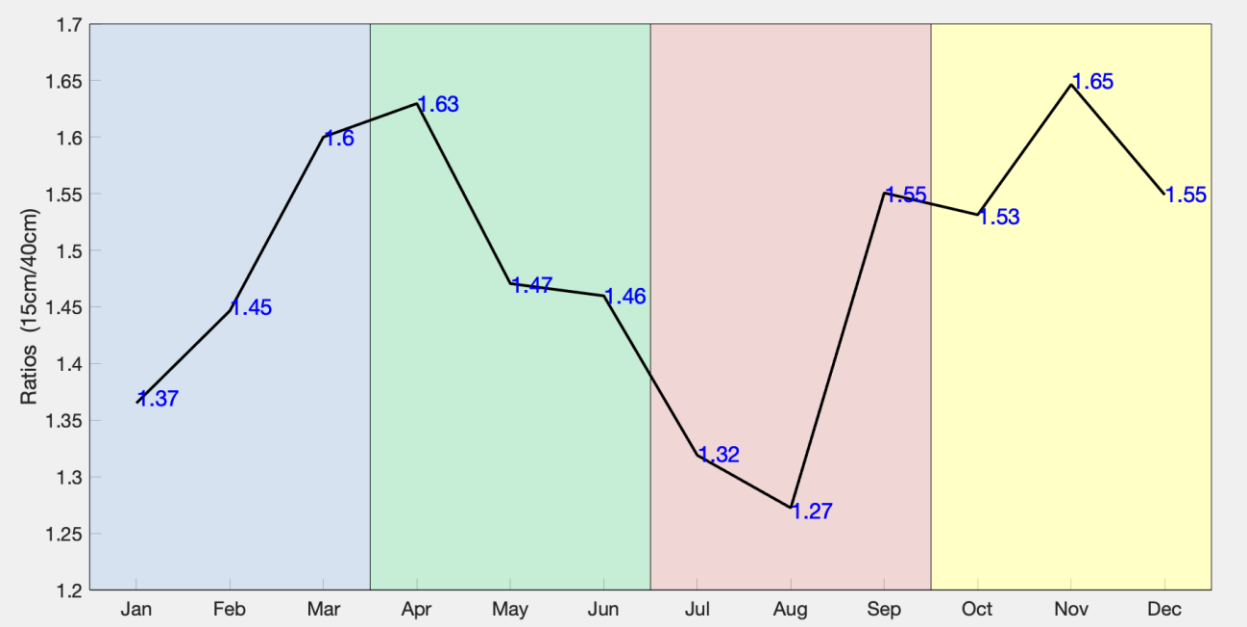

4) Line 393: this would be clearer if written as "be attributed to the different ways in which the two groups treated the data."

R: We agree and we include your recommendation in line 393.

5) Schmitz (2005) does not appear to be in the text and should be removed from the reference list.

R: We remove Schmitz (2005)

Effect of Caribbean Water Incursion into the Gulf of Mexico derived from Absolute Dynamic Topography, Satellite Data, and Remotely - sensed Chlorophyll-*a*

Authors:

Juan A. Delgado[1,2,5]; Joël Sudre [3], Sorayda Tanahara[1]; Ivonne Montes[4],

J. Martín Hernández-Ayón[5], Alberto Zirino[6]

Author affiliations:

[1]*Facultad de Ciencias Marinas, Universidad Autónoma de Baja California, Transpeninsular Tijuana-Ensenada, no. 3917, Fraccionamiento Playitas, CP 22860. Ensenada, Baja California, México.*

[2]*Instituto Tecnológico de Guaymas/ Tec. Nacional de México, Guaymas, Sonora, México.*

[3]*LEGOS, CNRS/IRD/UPS/CNES UMR 5566, 18 av. Ed Belin, 31401 Toulouse Cedex 9, France*

[4]*Insitituto Geofísico del Perú. Lima, Perú.*
[5]*Instituto de Investigaciones Oceanológicas, Universidad Autónoma de Baja California, Transpeninsular Tijuana-Ensenada, no. 3917, Fraccionamiento Playitas, CP 22860. Ensenada, Baja California, México.*
[6]*Scripps Institution of Oceanography, University of California, San Diego, 9500 Gilman Drive, La Jolla, California 92093, USA.*
Corresponding author: Sorayda Tanahara (stanahara@uabc.edu.mx)
Facultad de Ciencias Marinas
Universidad Autónoma de Baja California.

Key points:

Twenty-five years of satellite observations of absolute dynamic topography confirm the patterns of Caribbean water intrusion in the Gulf of Mexico.

Larger volumes of oligotrophic waters from Caribbean Sea are entering the western Gulf of Mexico and lowering the surface and near surface *Chl-a* concentration.

Abstract

The dynamics of the Loop Current (LC) and the detached Loop Current eddies (LCEs) dominate the surface circulation of the Gulf of Mexico (GoM) and transport Caribbean water (CW) into the gulf. In this work, 25-years (1993-2017) of daily satellite data are used to investigate the variability of these physical processes and their effect on chlorophyll-a (Chl-a) concentrations from 1998-2017 including temporal changes, mean differences, and regional concentration tendencies. Physical variables analyzed are absolute dynamic topography (ADT) and oceanic currents. From

the ADT and oceanic current monthly climatologies, it is shown that there is an annual intrusion of the CW with an inward incursion that starts in spring, peaks in the summer, reaches to 28˚N and 90.45˚W, and then retreats in winter to 26.5 ˚N and 88.3 ˚W, approximately. Minimum surface Chl-a concentrations (<0.08 $mg\ m^{-3}$) are found during the summer-autumn period inside the region of maximum incursion of the CW; the opposite is observed during the winter period when Chl-a concentrations were at a maximum, e.g., >0.14 $mg\ m^{-3}$. The three-year running averages of the ADT 40-cm isoline reproduce qualitatively the climatological pattern of 25 years showing that before 2002 the CW was less intrusive. This suggests that from 2003 onward, larger volumes of oligotrophic waters from Caribbean Sea have invaded the western GoM and reduced mean surface Chl-a concentrations. A direct comparison between the 1998-2002 and 2009-2014 periods indicates that in the latter time interval, Chl-a concentration above waters deeper than 250 *m* has decreased significantly.

1. Introduction

The effects of global warming on the circulation of the world's oceans and its concomitant consequences on the oceans' biological productivity are some of the most important scientific and economic issues of our times. Forecasting of the effects of global warming on the oceans' resources depends on having a clear understanding of the manner in which physical processes (e.g., solar radiation, winds, circulation and vertical mixing) affect primary production. This understanding is aided by the availability of remote sensing observations, unparalleled in their spatial and temporal coverage of the earth's surface. Since 1990, satellite data of absolute dynamic heights (ADT), Chlorophyll-a (Chl-a) concentration, and derived products (eddy kinetic energy (EKE), geostrophic and Ekman currents) have been available to study the Gulf of Mexico (GoM), an important socio-economic region for fisheries, petroleum, natural gas, and tourism. We have

availed ourselves of a 25-year time series of satellite data to study the relationship between the physical dynamics of the GoM and its effect on primary production in the context of a global warming scenario. Unlike previous studies, this work entails the analysis of the Loop Current (LC) and the LC eddies (LCEs) path footprint, and of the dominant features of the surface circulation that transport Caribbean Water (CW) into the GoM (Nowlin and McLellan, 1967; Morrison et al., 1983). The LC in the eastern GoM is part of the North Atlantic Ocean Subtropical Gyre, an essential contributor to the inter-hemispheric Meridional Overturning Cell (Schmitz and McCartney, 1993; Candela et al., 2003; Schmitz et al., 2005). This current carries warm waters from the gulf to the North Atlantic through the Florida Straits via the Gulf Stream (Hurlburt and Thompson, 1980), thereby also being an important contributor to the upper ocean heat budget of GoM (Liu et al., 2012). Based on a detailed analysis in the central and western GoM by Portela et al. (2018), within the Gulf are seven water masses in order of increasing mean density: remnants of the Caribbean Surface Water (CSWr: also referred to as CW), North Atlantic Subtropical Underwater (NASUW), Gulf Common Water (GCW), Tropical Atlantic Central Water (TACW), the nucleus of the (TACWn), Atlantic Intermediate Water (AAIW) and North Atlantic Depth Water (NADW). Here, we are principally concerned with surface effects.

CW enters in the GoM via the LC with specific biological (i.e., low Chl-a) and physical characteristics (warmer by ~0.6 units and less saline waters by ~0.5 units). The current penetrates into the gulf, reaching 28˚N, near the Mississippi Delta. As it extends to the north, it forms a loop (Austin, 1955) that turns southeast to ultimately exit into the Atlantic Ocean.

Knowledge of how the thrust of the LC affects the intrusion of CW is based on hydrographic data (Leipper, 1970; Niiler 1976; Behringer et al., 1977; Molinari et al., 1977; Huh et al., 1981; Paluszkiewicz et al., 1983), remote sensing observations (Vukovich et al.1979;

Vukovich, 1988; Leben and Born, 1993; Leben, 2005), and, in the last twenty years, by numerical modeling (Hurlburt and Thompson, 1980; Candela et al., 2003; Oey et al., 2005; Sturges and Lugo-Fernandez, 2005; Counillon and Bertino, 2009; Cardona and Bracco, 2016; Wei et al., 2016). More recently, novel developments based on artificial neural networks and empirical orthogonal function analysis have also been applied to predict LC variation (Zeng et al., 2015), effecting reliable forecasts for up to 5 to 6 weeks. Knowledge of how the primary forcing mechanism affects the loop current is important to the circulation of the GoM both as a direct and indirect generator of surface-layer eddies and as a source of lower-layer flows (Hamilton et al., 2016). Based on satellite altimetry observations and the dynamic height gradient from 1993 to 2009, Lindo-Atichati et al. (2013) observed northward seasonal penetration of the LC, peaking in summer. LC extension and anticyclonic eddy separation are the result of the momentum imbalance (Pichevin and Nof, 1997) and form the shape of future LCEs. Chang and Oey (2010) using a numerical model, proposed that the wind stress could be the primary forcing that releases LCEs. In a second paper, supported by satellite observations, they proposed that the LC intrusion and the shedding of the LCEs followed a biannual cycle (Chang and Oey, 2013). A reanalysis of archived data also detected statistically significant LCEs separation seasonality (Hall and Leben, 2016). Recently, Candela et al. (2019) analyzed four years of water current data and reported a seasonal cycle in the transport through the Yucatan channel with the annual cycle as the main harmonic peak in July.

Interacting seasonal and stochastic processes could trigger the separation of the LCEs (Fratantoni et al., 1998; Zavala-Hidalgo et al., 2003; Zavala-Hidalgo et al., 2006) as well as forming Caribbean eddies and other topographic features (Garcia-Jove et al., 2016). In this context, the LC system has some similarities with the North Brazil Current retroflection (Pichevin et al., 1999; Goni and Johns, 2001; Zharkov and Nof, 2010), the Agulhas retroflection (de Ruijter et al.,

111 1999; Baker-Yeboah et al., 2010) and with the Gulf Stream, where large meanders pinch off as
112 warm rings (Brown et al., 1983; Richardson, 1983; Savidge and Bane, 1999).

113 Despite extensive research, after more than a half-century we are still struggling to
114 completely understand LC variability, the processes controlling the loop current extension, and the
115 mechanism of detachment of anticyclones from the loop. Because positive time trends have been
116 reported in temperature, winds, sea level and the greater number of detached eddies separated from
117 the LC, it can be expected that these phenomena would affect primary productivity and, indirectly,
118 surface Chl-a concentration (Polovina, et al., 2008; Laffoley and Baxter., 2016). In this work, 25-
119 years (1993-2017) of daily ADT data combined with monthly radiance data from 1998-2017 are
120 used to investigate the variability of the transport of Caribbean surface water into the gulf and its
121 effect on Chl-a concentration. We examined temporal changes, mean differences, and regional
122 concentration tendencies.

123

124 **2. Data and Methods**

125 Three independent data sets were used to provide evidence of temporal variability in the extension
126 of CW into the GoM. We used ADT and surface velocity fields (geostrophy and Ekman) from the
127 GEKCO (Geostrophic Ekman Current Observatory, Sudre et al., 2013) product from 1993 - 2017
128 with a resolution of 0.25˚x0.25˚, in conjunction with *Chl-a* ocean color data derived from the
129 reprocessing R2014.0 product suite from Aqua MODIS (Moderate Resolution Imaging
130 Spectroradiometer) and from SeaWIFS (Sea-Viewing Wide Field of view Sensor), using the OCx
131 Algorithm with a spatial resolution of 9X9 km (https://oceancolor.gsfc.nasa.gov/cgi/l3). The 2003-
132 2017 monthly *Chl-a* ocean color product was derived from Aqua MODIS and the 1998-2002
133 monthly *Chl-a* ocean color product was derived from SeaWIFS.

Climatology was created from maps of ADT that result from the elevation of the sea surface height referenced to the geoid using the product from DUACS (Data Unification and Altimeter Combination System) available on the AVISO (Archiving, Validation and Interpretation of Satellite Oceanographic data) website https://www.aviso.altimetry.fr/en/data. The ADT climatology was constructed using the 25 years of daily satellite maps, from 1993 to 2017, averaging all the Januaries, Februaries … and Decembers. We considered LCEs in any stage of formation, detaching and reattaching to the LC as evidence of the incursion of the CW. After the ADT climatology was obtained, the predominant boundary contour of CW was extracted from each climatological month. It was observed that the 40 ±2.2 cm ADT contour was well matched to the climatological maxima of its respective EKE. For this reason, the ADT 40 cm contour is taken as the main ADT reference that tracks the Caribbean Water Front (CWF).

Specifically, monthly CWF positions were obtained from short-term running averages of daily satellite observations in three-year periods. Each running average was moved rearward by one year, e.g. 1993-1995, 1994-1996 … 2014-2016, 2015-2017. For each three-year period, a set of 12 monthly maps was obtained resulting in a total of 23 sets of monthly CWF maps: 10 sets from 1993 to 2002 and 13 sets from 2003 to 2017. We used the 40 cm contour of each set of three-year averages because this was the contour with the highest EKE observed in the 25-year data set. To retrieve the CWF contours, we first determined the initial latitudinal position of the CWF to be at 80.7^{o}W with the respective corresponding longitudinal positions between Cuba and Florida. The CWF contour lines that run from east to west and finish close to the tip of the Yucatan peninsula were separated by 0.2 ±0.1 degrees. However, some ADT contour "islands" appeared next to the CWF with a typical distance of > 0.3 degrees from the CWF contour. Additionally, a spectral analysis was done using a daily time series of 25 years of ADT data to build a spatially averaged

region influenced by the LC between 91.25°W, 23.125°N and 83.5°W, 28.12°N.

When ADT island distances were > 0.3 degrees from the front, we used a Matlab code procedure to eliminate them from the CWF contours. Once the CWF's contours were retrieved, the next step was to visually corroborate the quality and coherence of each CWF contour over the monthly field maps of ADT, sea surface currents, and *Chl-a* distribution. In this way, inconsistencies were detected and corrected. The Matlab code procedure satisfactorily corrected 91.3% of the contours. The remaining sets were corrected by hand via visual analysis.

Main mesoscale instabilities were obtained from calculations of the climatological monthly EKE maps of geostrophic and Ekman currents obtained from 25 years of daily satellite observations of GEKCO using following equation:

$$u = u' + U; \qquad u' = u - U$$

$$v = v' + V; \qquad v' = v - V$$

$$EKE = \tfrac{1}{2}\,(u'^2 + v'^2)$$

Where (u, v) is the total current ($u=u_E+u_g$ and $v= v_E+v_g$; (u_E, v_E), is the Ekman and (u_g, v_g) is the geostrophic current, U and V are the means of the oceanic currents and (u' and v') are the anomalies of the current. To find the relationship between ADT and EKE patterns, the 40 *cm* ADT isoline was overlaid on the monthly EKE maps. This made the EKE means representative of the energy of the mesoscale eddy field (Jouanno et al., 2012).

For consistency between the different satellite datasets, all monthly climatological spatial fields were standardized at 0.25˚x0.25˚ spatial resolution by bilinear interpolation.

3. Results and discussion

3.1. Tracking the Intrusion of Caribbean Water

The LC enters the gulf through the Yucatan Channel and exits through the Straits of Florida, penetrating northward into the GoM until instabilities form in the current and a ring-like LCEs pinches off. There are two ways of tracking the LC: 1) tracking the thermal signal (not possible in summer due to weak thermal contrast in the GoM), and 2) tracking the sea surface height trough the satellite altimetry. In 2005, Leben, using the 17 *cm* contour in the daily sea surface topography maps (this contour closely follows the edge of the high-velocity core of the LCEs and LC), tracked the LC thermal fronts in the sea surface temperature images during good thermal contrast. In a different way, Lindo-Atichati et al. (2013) calculated the maximum horizontal gradient of the sea surface height (SSH) to track only the contours of the LCF. In this work, we used the ADT to track both the LC and the LCEs formed by the influence of the CW. Monthly mean surface oceanic currents from GEKCO overplotted on the ADT data are shown in Fig. 1. Maximum satellite surface current velocities in the Caribbean Sea and the GoM, as well as in the Yucatan current on the continental coast, were > 50 $cm\ s^{-1}$, coinciding with *in situ* estimates of ~ 60 $cm\ s^{-1}$ (Badan et al., 2005). The monthly GoM total current fields show the variability of the primary forcing that coincides with the mean ADT edge; the vectors of maximum velocity are tangent to the edge of the maximum slope change. To locate the CW, the 40 *cm* mean ADT's isoline was chosen. The ADT reference corresponds to regions of maximum gradients of ADT and maximum EKE. Fig. 1 shows that (mostly) in autumn (October, November and December) and winter (January, February and March), the CW retracts to its most southeasterly location. In contrast, in spring (April, May, June) and summer (July, August, September), CW penetration moves towards the northwest. In fact, the extension begins in May and reaches maximum penetration in August, showing an annual

pattern. This movement is similar to that observed by Chang and Oey (2013). They found that in summer, the maximum LC intrusion was forced by the trade winds. Their and our observations are also consistent with the work of Candela et al. (2019) who reported that water transport into the GoM in July through the Yucatan channel was at a maximum.

It is accepted that the LCEs occur in a geographical control zone that is based on momentum imbalance (Pichevin and Nof, 1997; Nof, 2005) rather than instability. Also, we should not abandon the idea that the formation of instabilities such as meanders and cyclonic eddies are due to high EKE produced by upstream conditions that influence the circulation within the GoM (Oey et al., 2003) and produce changes in the fluxes in the Yucatan Channel (Candela et al., 2002), transport variations in the LC (Maul and Vukovich, 1993), variations in the deep outflow (Bunge et al., 2002), and cyclonic eddies in Campeche Bank and Tortugas (Fratantoni et al., 1998; Zavala-Hidalgo et al., 2003). The areas of large EKE are related to the intrusion and retreat of CW (Garcia-Jove et al., 2016) via baroclinic and barotropic instabilities (e.g. Jouanno et al., 2009).

Fig. 2 shows that the 40 *cm* isoline encloses the maximum EKE area of the LC-LCEs during each climatological month, demonstrating that its distribution is mainly centered in the LC region; consequently, the maximum EKE borders the CW front just where the abrupt horizontal gradients of ADT exist and changes of current speed occur. It is clear that the 40 *cm* isoline of ADT matches very well both the maximum EKE values and the maximum ADT gradient and is a good tracker of the contours of LC-LCEs. Lindo-Atichati et al. (2013) proposed a methodology using the SSH maximum horizontal gradient, which is the addition of sea height anomaly and mean dynamic topography, to obtain the contours of LCF and the LCEs. In our analysis, we chose the 40 *cm* isoline as a general reference to track both LCF and LCEs, and CW transport.

The enhanced monthly EKE signals respond in the same way as the LCF, repeating the

mean monthly pattern as well as the total currents; the CW intrusion starts in spring and peaks in summer to retract in autumn and winter, and there are no relevant mesoscale EKE's structures in the western GoM. These results confirm an annual pattern of CW intrusion in summer months and retraction in winter.

3.2 West and Northward Caribbean water extension

The monthly intrusions of the CWF were tracked by taking as a reference the northernmost latitudes and westernmost longitudes of the 40 *cm* ADT isoline representing 1993-2017 monthly average values of the ADT (not spatially averaged). The climatological position of the CWF for each month of the year is shown in Figure 3. These results confirm the annual intrusion of the CW as follows: 1) Analysis of the maximum north and westward penetration of the front over 25 years shows that from January to February, it is retracted southeast to ~ 26.55˚N and ~ 88.32˚W (Fig. 3a and 3b, respectively), and intrudes to 28˚N, 90.45˚W in August; 2) an ADT spectral analysis derived from 25 years of daily data from the CWF region shows a strong annual signal that originates from the back and forth of the ADT signal (Fig. 3c). In this work, the ADT signal also includes the seasonal steric effect. Based on Hall and Leben (2016), a steric signal appears as an annual sine wave with 5.8 cm amplitude. When the estimated seasonal steric influence is removed, the high energy peak diminishes by 74%.

In winter, the "tongue" of the CWF moves slowly to the north without westward advance; in spring it lengthens and travels slightly towards the west. From January to March, the northward CWF position shifts slowly, tracing a gently sloping line, that starts at 26.5˚N, reaches its maximum northern position of 28˚N in August, and then decreases in December to 26.28˚N (maximum travel of the CWF was 1.72˚ or 191 *km)*. In summer, the CWF intrudes further into the

interior of the GoM both in the north and west: its maximum northern and westward advance occurs in August to 28˚N and 90.45˚W, but then the CWF retracts in the last month of summer. Regarding CWF´s westerly movement (Fig. 3b), the CWF traveled little from January to April; in May however, it extended quickly and in July, August, and September reached approximately 90.2˚W, and peaked in October at 90.76 ˚W (maximum range was 2.56˚ or 253 *km*, calculated at 27.5˚N latitude). In December, the CWF retracted abruptly to 88.24˚W.

Another aspect of the CWF is the rate of intrusion and retraction. From March to August, the CWF moves to the north with a penetration speed on the order of ~ 1.02 *km day*$^{-1}$, covering a distance of 153 *km or* 1.37˚. On the other hand, the rate of retraction from August to November is ~ 1.86 *km day*$^{-1}$, equivalent to *168 km (1.51˚).* The entire process of northerly intrusion occurred in three stages: first, from January to April, the front moved slowly northward, increasing its speed while maintaining its westward position. Between May and July the front moved northwest; then was quasi-stationary in July and August, near 90.45˚W; finally, in September, it moved from 90.13˚W to 90.76˚W, equivalent to 63 *km* at a rate of 2.1 *km day*$^{-1}$. The retraction to the west occurred relatively quickly as the front retracted 193 *km* towards the east in a single month (October) at the rate of 6.3 *km day*$^{-1}$, and in November traveled 41 *km* at a rate of 1.4 *km day*$^{-1}$, also towards the east.

Fig. 4 shows the calculated climatological areas of standard deviation (STD) of the CWF contours > 15 cm (dotted line) and CWF contours > 40 cm (heavy black line). From these areas we calculated ratios between the two (15cm/40cm). The STD contour of 15 cm was selected because this value was three times greater than the annual steric signal reported by Hall and Leben (2016). Ratio values were 1.37 in January, increased to 1.45 in February, and to 1.60 in March, then peaked in April (1.63) to decrease in May (1.47) and June (1.46), reaching a low value in

August (1.27). The monthly ratio then increased in September to 1.55, decreased slightly in October (153), reached a maximum value in November to 1.65, and settled to 1.55 in December. A plot of these monthly ratios clearly shows a strong biannual signal peaking in April and November (not pictured). Chang and Oey (2012, 2013) proposed that the LC intrusion and the shedding of the LCE followed a biannual cycle. This biannual cycle can also be related to the annual lowest and highest values of the ratio.

3.3 Monthly Spatial Variability of the Caribbean Water Front

It was found that where penetration-retraction of the CWF occurs, STD variability varies from 15 to 35 *cm*, extending west to 90.8°W in winter and 93.5°W in summer (Fig. 4). West of the CWF, in the deep zone of the GoM, the observed variability was close to 10 *cm* distributed in the band of latitude between 23˚N and 28.5˚N. The regions of maximum variability (STD > 15 *cm*) occur in the CWF zone and extend outside the irregular area of reference (isoline of the 40 *cm* ADT). The effect of CWF penetration and regions of anticyclonic circulation was determined from the area of the variability of ADT, with maximum values close to ~35 *cm* in the central region of the CWF, at 86.67˚W and 25.6˚N. The percentage of the area of influence of STD > 15 *cm* in relation to the area of the gulf (1.56×10^6 km^2) is presented in Fig. 5, where a gradual monthly increase is observed from January to October, followed by a decrease in November and December. In January, the direct influence of the CWF on the gulf by area was 12.4%, rising to 21.5% for October, to subsequently decrease in December to 15.4%. We suppose that the greater percentage area of the STD may be attributed to a greater influence of Caribbean Sea water.

3.4 Changes in the Caribbean Water Incursion from 2003 to the Present

Using the 40 *cm* reference, a 3-year running average of the ADT data was calculated to extract the

minimum number of years that would produce a similar pattern over a quarter century of the CWF. The results indicate a difference in CWF path and westward penetration before and after 2002. It is observed that before 2002 the CWF was less intrusive in the west (Fig. 6), after 2002 it extended towards the west in both summer and autumn (Fig. 7). It is important to note that the intrusion of the CWF is due to the influence of LCEs that have a strong presence in the western GoM. This fact is supported by a statistical analysis of the lifetimes of the LCEs during two time periods (1993-2002 and 2003-2015) (http://www.horizonmarine.com/loop-current-eddies.html). The data shows that the LCEs in the 1993-2002 period had a mean life of 6.8 months while the average life in 2003-2015 was 11.7 months. To prove that there is significant difference between these periods, a student-*t* test was applied with the result that the difference between them is significant ($t = -3.098$, $p = 0.005$). The LCE mean life difference is clear evidence that the incoming volume of water from Caribbean Sea (with oligotrophic features, Aguirre –Gómez and Salmerón-García, 2015) has reached farther in the western GoM after 2002. These observations also agree with the results of Lindo-Atichati et al. (2013), confirming that, on average, the LC northward intrusion starts to increase in 2002. These authors also report an increase in number/year of LC rings over the same period that also coincided with a significant increase in sea height residuals (2.78 ± 0.26 cm/decade from 1993–2009). This supports the finding that from 2003 onward, larger volumes of oligotrophic waters from Caribbean Sea have invaded the western GoM.

3.5 Chlorophyll-a Satellite Imagery, Climatology, and Changes in the Last Decade

Another product that tracks the effect of CW inside the western GoM is the *Chl-a* satellite imagery, being an index of primary productivity (Boyer et al., 2009). Physical processes that affect the distribution and abundance of *Chl-a* include estuarine influxes, depth of the nutricline, wind stress, thermal stratification and eddy advection. However, over deep waters of the GoM, it is the wind

315 stress and the thermal stratification that principally affect the *Chl-a* concentration (Martínez-López
316 and Zavala-Hidalgo, 2009; Müller-Karger et al., 2015, Damien et al., 2018). It was found that the
317 oligotrophic CW contrasts seasonally with the gulf waters and allows the observation of two levels
318 of *Chl-a* (high and low, Müller-Karger et al., 1989). Here, the temporal relationship between the
319 CWF and *Chl-a* concentration was constructed from SeaWifs and MODIS monthly climatological
320 images (Fig. 8). The highest concentrations of *Chl-a* in the interior of the GoM are observed during
321 autumn and winter months when high concentrations are triggered by vertical mixing (Pasqueron
322 de Fommervault et al., 2017; Damien et al., 2018) when values were > 0.14 $mg\ m^{-3}$ in agreement
323 with Dandonneau et al. (2004), whereas in spring-summer they decreased to 0.08 - 0.09 $mg\ m^{-3}$.
324 During spring-summer, when the maximum CW penetration occurs, our data confirms that the
325 "footprint" of the CWF water (delineated by the 40 *cm* isoline of ADT) is in general oligotrophic
326 indicating that Caribbean water has indeed entered the GoM. During this period, the *Chl-a* surface
327 concentration remains low as the increase in surface temperature strengthens stratification.
328 Additionally, the winds from the southeast are weak, thereby reducing the mixing of nutrients to
329 the surface. In contrast, during the autumn-winter months, the northerly winds are stronger,
330 increasing vertical mixing, deepening the mixed layer, and carrying cold, nutrient-rich subsurface
331 water into the euphotic layer (Müller-Karger et al., 1991; Müller-Karger et al., 2015; Pasqueron
332 de Fommervault et al., 2017).

333 In seeking relationships between the spatial-seasonal distribution of the *Chl-a*
334 concentration and the incursion signaled by the ADT-generated data, three spatial-temporal
335 periods were selected, each was averaged pixel by pixel, and the three were labeled: "early" (1998-
336 2002), "middle" (2003-2008), and "contemporary" (2009-2014) epochs. The 5-year averages of
337 the "early" and "contemporary' periods of two separate areas were compared: 1) an area located in

the western GoM at 95.5˚W, 22.12˚N and 91.5˚W, 25.87˚N, and 2) a smaller area located in the center of the LC at 86˚W, 22.12˚N and 84.75˚W, 23.37˚N (Fig. 9). The differences in the means were tested for significance with a 2-tailed z test at the 95% confidence level (Fowler et al., 2013). The results are shown in Table 1 and may be summarized as follows:

A. Temporal differences: 1) Western GoM differences between early and contemporary *Chl-a* concentrations are significantly different in all seasons; 2) Loop Current differences between Early and Contemporary *Chl-a* concentrations are significantly different during winter, spring, and autumn, but not in summer;

B. Spatial differences: 1) In winter, the Western GoM is significantly higher in *Chl-a* than the LC during both early and contemporary periods; 2) In the spring, the Western GoM is significantly higher than the LC during the early period, but not in contemporary period; 3) In summer, the LC is significantly higher than Western GoM during both early and contemporary periods; 4) In autumn, the Western GoM is significantly higher than LC during the "early" period but not significantly different from the LC in the contemporary period.

C. Seasonal Differences. In the Western GoM and the LC in both the early and contemporary periods, *Chl-a* decreases from winter to spring and from spring to summer, and increases from autumn to winter, but autumn concentrations do not exceed winter (See also Fig.9). All differences are significant.

Examination of Table 1 indicates that at both areas, the winter season is most productive, followed by autumn, with the lowest *Chl-a* concentrations occurring in summer (see also Fig. 9). There is also a time-dependent trend, with contemporary values that are, in general, lower than the values in the early and middle epochs. Both areas exhibit identical climatic trends over time and

during each season, indicating that these effects are applicable outside of the continental shelf. The early spring epoch is more eutrophic than the middle and contemporary epochs, indicating a decline in nutrient concentrations over time. This effect is also evident in the LC core, where *Chl-a* concentrations decreased with time and signals the entrance to the gulf of more oligotrophic water during the middle and contemporary epochs. Perhaps the most notable seasonal scenario occurs in the summer to early October period, when the CWF "tongue" extends in the interior of the GoM. Although the concentration of *Chl-a* in the Western GoM declines gradually with time to from ~ 0.09 to ~ 0.08 $mg\ m^{-3}$, the interesting fact is that the area of oligotrophic water expands and become larger in the contemporary period. On the other hand, in the LC core, the *Chl-a* concentrations in the three epochs do not significantly differ, suggesting that the water entering the GoM is from a single source, namely, the Caribbean Sea. In general, the extensive penetration of the LC within the GoM, as well as the increase in the life periods and sizes of LCEs coincide with the intrusion of nutrient-poor CW.

Two points summarize the result of the seasonal analysis of the three epochs: First, the extent of the CW intrusion confirms the north-west migration of eddies during each epoch, second, the *Chl-a* concentration declines over time.

The second point was confirmed by calculating the average *Chl-a* concentrations outside the continental shelf over two time periods, considering only the concentrations above waters deeper than 250 *m*. Using data from 1998 to 2002 (SeaWIFS), and from 2009 to 2014 (MODIS) we conducted a student-t test for difference in the means (Fig. 10). The latter period was significantly lower with $t = 4.75$ and $p<0.001$ ($n_1 = 1{,}825$; $n_2 = 2{,}190$). This analysis confirms that the *Chl-a* concentration of the GoM decreases over time and appears to disagree with the results of Müller-Karger et al. (2015) who did not indicate a time trend in *Chl-a* concentration in the GoM.

As the data were taken with different sensors and to eliminate the uncertainty that this difference is not caused by a systematic difference between the SeaWIFS and MODIS data sets used in our analysis, we calculated least square regressions to the SeaWIFS and MODIS time series at four stations corresponding to the northwest, northeast, southwest and southeast regions of Müller-Karger et al. (2015) (Fig. 11). For each data set, inner slopes as well as overall slopes were calculated. For all four stations, the SeaWIFS (1998-2002) and the MODIS (2003-2017) data series merged exactly and all stations show negative trends; equivalently, the combined time series (1998-2017) also show a negative tendency, supporting the conclusion that the *Chl-a* concentrations over the deep GoM has decreased over time.

The difference between our results and those obtained by Müller-Karger et al. (2015) may be attributed to the different way in which the two groups treated the data. Müller-Karger et al. (2015) divided the GoM into 4 quadrants with depths of over 1000 m: Region 1-North East (RO1), Region 2 (RO2 -Northwest), Region 3 (RO3-Southeast), and Region 4 (RO4 Southwest) and calculated the spatial average in each quadrant to build four-time series, from 1993 to 2012. In their words, "Time series of anomalies of wind speed, SST, SSHA and *Chl-a* concentration were obtained by subtracting the monthly mean (climatology) from the monthly field for that variable". Time series of wind speed, sea surface temperature (SST), sea-surface height (SSH), and *Chl-a* data obtained at these stations from satellite products was analyzed statistically, and plotted. Other variables plotted by Müller-Karger et al. (2015) were mixed layer depth (MLD) as calculated from a hydrodynamic model, and net primary production (NPP) calculated from MODIS data using the vertically generalized productivity model (VGPM) of Behrenfeld and Falkowski (1997).

On the other hand, we calculated the average of the *Chl-a* concentration pixel by pixel in waters over 250 m depth, for two time periods (1998-2002 and 2009-2014), and subtracted the

406 respective monthly (climatological) means to find the difference (Fig. 10). From 2009 onward, the
407 difference indicated a small reduction of *Chl-a* in the first optical depth (1-20 or 40 meters of
408 depth) that is increasing with time. A student-t test was used to conclude that the reduction was
409 significant. We also treated the data exactly as did and Müller-Karger et al. (2015) obtained slightly
410 negative slopes Müller-Karger et al. (2015) over the entire 1998 to 2013 period.

411 We suggest that Müller-Karger et al. (2015) did not detect the small negative trend in their
412 *Chl-a* plots because their calculated slopes indicated no time-dependent change. We surmise that
413 they were also influenced by the lack of slope in the modeled MLD plot, despite clear, positive,
414 trends for SST, SSHA, and wind force. Actually, although close to zero, the slopes, as indicated
415 in Müller-Karger et al. (2015) were not zero, but -0.03 for RO1, -0.01 for RO2, and simply given
416 in as -0.0 for RO3 and 0.0 for RO4 (see their Table 1). Müller-Karger et al. (2015) also ignored
417 the fact that the time-*Chl-a* correlation coefficients (R) for all four regions was negative.

418 To confirm our findings, we chose 4 stations, each one centrally located in each quadrant
419 (Müller-Karger et al., 2015), and conducted regression analyses of the logarithmic transform of
420 the SeaWifs and MODIS *Chl-a* concentrations. All four regions showed a negative slope, a
421 negative R, and the negative slopes in the southern gulf (RO3 and RO4) were significantly different
422 from 0 ($p << 0.05$). This is shown in Fig. 11.

423 The observed small, but persistent decline in *Chl-a* from 1993 to 2017 may be attributed
424 to the AMOC's over-all effect of warming the surface water and thereby promoting stratification.
425 However, we wish to make clear that our conclusion about the recent time-dependent lowering of
426 the *Chl-a* pertains only to the near surface, and may not indicate a decrease in the primary
427 productivity integrated over the entire water column. In the GoM, the chlorophyll maximum as
428 measured by fluorescence occurs at about 75 m, e.g., below one optical depth, and is greater in

summer than in winter (Pasqueron de Fommervault et al., 2017), indicating that the relationship between water column productivity and near surface *Chl-a* concentration in the GoM requires further study. Our own results and conclusions are based on SeaWifs and AquaMODIS chlorophyll data, which in Type One water**,** correlate very well with chlorophyll measured with standard laboratory methods (Mati Kahru, personal communication). In our work we can only say that according to these satellite products, we find a time-dependent diminution of the Chl-a signal. This diminution has been widely observed by others although in other waters (Behrenfeld et al., 2006, Polovina et al., 2008; Irwin and Oliver, 2009, Laffoley and Baxter., 2016).

4. Summary and conclusions

The availability of a large spatial extension of satellite observations of ADT, sea surface currents, wind stress over a quarter of century and Chl-a over 20 years has enabled us to confirm the LC and CW dynamics observed in the 60's and 70's with more recent *in situ* observations. The verification of the CWF climatologies developed in this work is important as a reference baseline for further numerical modeling, and it impacts assessments of the gulf's biogeochemistry, energy, heat transport, and Chl-a concentration. A recent committee of the National Academic of Sciences, (2018) suggested three main study topics to advance the knowledge of the processes that characterize the GoM: 1) the LC system active area, 2) the variation of the inflows of the LC system, and 3) the dynamic interactions of the LC system in the west. Following these suggestions, we have confirmed that the maximum influence of the CW into the GoM (e,g., its maximum extension into the gulf or intrusion) has a temporal variability, being stronger in summer and weaker in the late fall and winter. This is supported by the fact that the generated monthly EKE maps have the maximum gradient at the periphery of the CWF and have a similar monthly pattern

of extension and retraction as the CWF.

We noted that in the summer months the wind stress from the southeast is weak, thereby minimizing the flow of nutrients to the surface and causing Chl-a to be low, specifically for three reasons: 1) The increase in the surface temperature of the water column strengthens stratification 2) The intrusion of the CW to the western gulf´s surface thickens the surface layer, and 3) The eddy-driven anticyclonic circulation deepens the nutricline. This contrasts with the cold seasons, when the surface temperature of the water is lower and the northerly winds are stronger, favoring the flow of nutrients to the surface.

The three-year running averages of ADT 40 cm isoline reproduce qualitatively the climatological pattern of a quarter of a century showing that before 2002 the CWF was less intrusive and the LCEs sizes were smaller. In the 1993-2002 period, we calculated that the mean life cycle of the eddies was 6.8 months and that in the 2003-2015 period the mean life cycle was 11.7 months. This difference suggests that after 2003, larger volumes of oligotrophic waters from Caribbean Sea have invaded the western GoM and reduced mean surface Chl-a concentrations. This work shows that

- The intrusion of the CW by LC-LCEs extends further into the western GoM than was previously known.
- *Chl-a* concentrations respond to the dynamics inside the GoM and are influenced by the CWF and the LC anticyclonic and cyclonic eddies.
- Since 2002, near surface *Chl-a* concentrations over bathymetry deeper than 250 m have decreased, and GoM surface waters may be turning more oligotrophic than in the

previous decade.

This work, based on 25 years of remotely sensed data, emphasizes the role of climatology in determining GoM circulation and its productivity and suggests that further climatologically-induced changes are probably imminent.

5. Acknowledgements

We thanks the reviewers for their positive criticisms and comments that help us to improve the manuscript. This study was carried out as part of the PhD thesis research conducted by the lead author at the Faculty of Marine Science and the Oceanographic Research Institute (FCM-IIO / UABC), Postgraduate Coastal Oceanography Program, and it was supported by the Graduate Professional Development Mexican Program grants (PRODEP: DSA/103.5/16/5801), the National Institute of Technology of Mexico (TecNM) and the Mexican Energy Bureau and Hydrocarbons Mexican Trust, project 201441. This is a contribution of the Gulf of Mexico Research Consortium (CIGoM).

6. References

Aguirre-Gómez, R. and Salmerón-García, O.: Characterization of the western Caribbean Sea waters through in vivo chlorophyll fluorescence, Rev. Mar. Cost., 7, 9–26, https://doi.org/10.15359/revmar.7.1, 2015.

Austin, G. B.: Some recent oceanographic surveys of the Gulf of Mexico, EOS, Transactions American Geophysical Union, 36(5), 885-892, https://doi.org/10.1029/TR036i005p00885, 1955.

Badan, A., Candela, J., Sheinbaum, J., and Ochoa, J.: Upper-layer circulation in the approaches to Yucatan Channel. In: W. Sturges and A. Lugo-Fernandez (Eds.), New Developments in the Circulation of the Gulf of Mexico, Geophysical Monograph Series, 161, 57-69, 2005.

Baker-Yeboah, S., Byrne, D. A., and Watts, D. R.: Observations of mesoscale eddies in the South Atlantic Cape Basin: Baroclinic and deep barotropic eddy variability, Journal of Geophysical Research, 115, C12069, https://doi.org/10.1029/2010JC006236, 2010.

Behrenfeld, M. J., and Falkowski, P. G.: Photosynthetic rates derived from satellite-based chlorophyll concentration, Limnology and Oceanography, 42(1), 1-20, 1997.

Behrenfeld, M. J., O'Malley, R. T., Siegel, D. A., McClain, C. R., Sarmiento, J. L., Feldman, G. C., … Boss, E. S.: Climate-driven trends in contemporary ocean productivity. Nature, 444(7120), 752–755. https://doi.org/10.1038/nature05317, 2006.

Behringer, D. W., Molinari, R. L., and Festa, J. F.: The Variability of Anticyclonic Current Patterns in the Gulf of Mexico, Journal of Geophysical Research, 82(34), 5469-5476, https://doi.org/10.1029/JC082i034p05469, 1977.

Boyer, J. N., Kelble, C. R., Ortner, P. B., and Rudnick, D. T.: Phytoplankton bloom status: Chlorophyll- a biomass as an indicator of water quality condition in the southern estuaries of Florida, USA, Ecological Indicators, 9(6), S56–S67,

https://doi.org/10.1016/j.ecolind.2008.11.013, 2009.

Brown, O. B., Olson, D. B., Brown, J. W., and Evans, R. H.: Satellite infrared observations of the kinematics of a warm-core ring, Marine and Freshwater Research, 34(4), 535-545, https://doi.org/10.1071/MF9830535, 1983.

Bunge, L., Ochoa, J., Badan, A., Candela, J., and Sheinbaum J.: Deep flows in the Yucatan Channel and their relation to changes in the Loop Current extension, Journal of Geophysical Research, 107(C12), 1–7, https://doi.org/10.1029/2001JC001256, 2002.

Candela, J., Ochoa, J., Sheinbaum, J., López, M., Pérez-Brunius, P., Tenreiro, M., … Arriaza-Oliveros, L.: The Flow through the Gulf of Mexico. Journal of Physical Oceanography, 49(6), 1381–1401. https://doi.org/10.1175/JPO-D-18-0189.1, 2019.

Candela, J., Sheinbaum, J., Ochoa, J., Badan, A., and Leben, R.: The potential vorticity flux through the Yucatan Channel and the Loop Current in the Gulf of Mexico, Geophysical Research Letters, 29(22), 2059, https://doi.org/10.1029/2002GL015587, 2002.

Candela, J., Tanahara, S., Crepon, M., Barnier, B., and Sheinbaum, J.: Yucatan Channel flow: Observations versus CLIPPER ATL6 and MERCATOR PAM models, Journal of Geophysical Research: Oceans, 108(C12), 3385, https://doi.org/10.1029/2003JC001961, 2003.

Cardona, Y., and Bracco, A.: Predictability of mesoscale circulation throughout the water column

in the Gulf of Mexico, Deep Sea Research Part II: Topical Studies in Oceanography, 129, 332-349, https://doi.org/10.1016/j.dsr2.2014.01.008, 2016.

Chang, Y. L., and Oey, L. Y.: Why does the Loop Current tend to shed more eddies in summer and winter? Geophysical Research Letters, 39(5), 1–7. https://doi.org/10.1029/2011GL050773, 2012.

Chang, Y.-L., and Oey, L.-Y.: Eddy and Wind-Forced Heat Transports in the Gulf of Mexico. Journal of Physical Oceanography, 40(12), 2728–2742. https://doi.org/10.1175/2010JPO4474.1, 2010.

Chang, Y.-L., and Oey, L.-Y.: Loop Current Growth and Eddy Shedding Using Models and Observations: Numerical Process Experiments and Satellite Altimetry Data. Journal of Physical Oceanography, 43(3), 669–689. https://doi.org/10.1175/JPO-D-12-0139.1, 2013.

Counillon, F., and Bertino, L.: High-resolution ensemble forecasting for the Gulf of Mexico eddies and fronts, Ocean Dynamics, 59(1), 83–95, https://doi.org/10.1007/s10236-008-0167-0, 2009.

Damien, P., Pasqueron de Fommervault, O., Sheinbaum, J., Jouanno, J., Camacho-Ibar, V. F., and Duteil, O.: Partitioning of the Open Waters of the Gulf of Mexico Based on the Seasonal and Interannual Variability of Chlorophyll Concentration, Journal of Geophysical Research: Oceans (March), 1–23, https://doi.org/10.1002/2017JC013456, 2018.

564 Dandonneau, Y., Deschamps, P. Y., Nicolas, J. M., Loisel, H., Blanchot, J., Montel, Y., Thieuleux,
565 F., and Bécu, G.: Seasonal and interannual variability of ocean color and composition of
566 phytoplankton communities in the North Atlantic, equatorial Pacific and South Pacific, Deep Sea
567 Research Part II: Tropical Studies in Oceanography, 51(1–3), 303–318,
568 https://doi:10.1016/j.dsr2.2003.07.018, 2004.
569
570 de Ruijter, W. P.M., Biastoch, A., Drijfhout, S. S., Lutjeharms, J. R. E., Matano, R. P., Pichevin,
571 T., van Leeuwen, P. J., and Weijer, W.: Indian-Atlantic interocean exchange: Dynamics,
572 estimation and impact, Journal of Geophysical Research: Oceans, 104(C9), 20885-20910,
573 https://doi.org/10.1029/1998jc900099, 1999.
574
575 Fowler, J., Cohen, L., and Jarvis, P.: Practical statistics for field biology, John Wiley & Sons, 2013.
576
577 Fratantoni, P. S., Lee, T. N., Podesta, G. P., and Müller-Karger, F.: The influence of Loop Current
578 perturbations on the formation and evolution of Tortugas eddies in the southern Straits of Florida,
579 Journal of Geophysical Research: Oceans, 103(C11), 24759-24779,
580 https://doi.org/10.1029/98JC02147, 1998.
581
582 Garcia-Jove, M., Sheinbaum, J., and Jouanno J.: Sensitivity of Loop Current metrics and eddy
583 detachments to different model configurations: The impact of topography and Caribbean
584 perturbations, Atmosfera, 29(3), 235–265, https://doi.org/10.20937/ATM.2016.29.03.05, 2016.
585
586 Goni, G. J., and Johns, W. E.: A census of North Brazil Current rings observed from

TOPEX/POSEIDON altimetry: 1992–1998, Geophysical Research Letters, 28(1), 1-4, https://doi.org/10.1029/2000GL011717, 2001.

Hall, C. A., and Leben, R. R.: Observational evidence of seasonality in the timing of loop current eddy separation. Dynamics of Atmospheres and Oceans, 76, 240–267. https://doi.org/10.1016/j.dynatmoce.2016.06.002, 2016.

Hamilton, P., Lugo-Fernández, A., and Sheinbaum, J.: A Loop Current experiment: Field and remote measurements, Dynamics of Atmospheres and Oceans, 76, 156-173, https://doi.org/10.1016/j.dynatmoce.2016.01.005, 2016.

Huh, O. K., Wiseman, W. J. J., and Rouse, L. J.: Intrusion of loop current waters onto the West Florida continental shelf, Journal of Geophysical Research, 86(C5), 4186–4192, https://doi.org/10.1029/JC086iC05p04186, 1981.

Hall, C. R. and Leben, R.R., 2016. Observational Evidence of Seasonality in the timing of Loop Current eddy separation, Dynamics of Atmosphere and Oceans 76,240-367.

Hurlburt, H. E., and Thompson, J. D.: A numerical study of loop current intrusions and eddy shedding, Journal Physical Oceanography, 10(10), 1611–1651, https://doi.org/10.1175/1520-0485(1980)010<1611:ansolc>2.0.co;2, 1980.

Irwin, A. J., and Oliver, M. J.: Are ocean deserts getting larger? Geophysical Research Letters,

610 36(18), L18609. https://doi.org/10.1029/2009GL039883, 2009.
611
612 Jouanno, J., Sheinbaum Pardo, J., Barnier, B., Molines, J. M., and Candela Pérez, J.: Seasonal and
613 interannual modulation of the Eddy Kinetic Energy in the Caribbean Sea, Journal of Physical
614 Oceanography, 42(11), 2041-2055. doi: 10.1175/JPO-D-12-048.1, 2012.
615
616 Jouanno, J., Sheinbaum, J., Barnier B., and Molines, J. M.: The mesoscale variability in the
617 Caribbean Sea. Part II: Energy sources, Ocean Modelling., 26(3–4), 226–239,
618 https://doi.org/10.1016/j.ocemod.2008.10.006, 2009.
619
620 Laffoley, D., and Baxter, J. M.: Explaining Ocean Warming: Causes, scale, effects and
621 consequences, Full Report. Gland, Switzerland: IUCN, 27,
622 https://doi.org/10.2305/IUCN.CH.2016.08.en, 2016.
623
624 Leben, R. R.: Altimetry-derived Loop Current metrics, In Circulation of the Gulf of Mexico:
625 Observations and Models, Geophysical Monograph Series, 161, edited by W. Sturges, and A.
626 Lugo-Fernandes, pp. 181–201, AGU, Washington, D. C., 2005.
627
628 Leben, R. R., and Born, G. H.: Tracking Loop Current eddies with satellite altimetry, Advances in
629 Space Research, 13(11), 325-333, https://doi.org/10.1016/0273-1177(93)90235-4,1993.
630 Leipper, D. F.: A sequence of current patterns in the Gulf of Mexico, Journal of Geophysical
631 Research, 75(3), 637-657, https://doi.org/10.1029/JC075i003p00637, 1970.
632

633 Lindo-Atichati, D., Bringas, F., and Goni, G.: Loop Current excursions and ring detachments
634 during 1993-2009, International Journal of Remote Sensing, 34(14), 5042–5053,
635 https://doi.org/10.1080/01431161.2013.787504, 2013.
636
637 Liu, Y., Lee, S.-K., Muhling, B. A., Lamkin, J. T., and Enfield, D. B.: Significant reduction of the
638 Loop Current in the 21st century and its impact on the Gulf of Mexico, Journal of Geophysical
639 Research, 117, C05039, https://doi.org/10.1029/2011JC007555, 2012.
640
641 Martínez-López, B., and Zavala-Hidalgo, J.: Seasonal and interannual variability of cross-shelf
642 transports of chlorophyll in the Gulf of Mexico, Journal of Marine Systems, 77(1–2), 1–20,
643 https://doi.org/10.1016/j.jmarsys.2008.10.002, 2009.
644
645 Maul, G. A., and Vukovich, F. M.: The relationship between variations in the Gulf of Mexico Loop
646 Current and Straits of Florida Volume Transport, Journal of Physical Oceanography, 23(5), 785–
647 796, https://doi.org/10.1175/1520-0485(1993)023<0785:TRBVIT>2.0.CO;2, 1993.
648
649 Molinari, R. L., Baig, S., Behringer, D. W., Maul, G. A., and Legeckis, R.: Winter intrusions of
650 the Loop Current, Science, 198(4316), 505-507, https://doi.org/10.1126/science.198.4316.505,
651 1977.
652 Morrison, J. M., Merrell Jr, W. J., Key, R. M., and Key, T. C.: Property distributions and deep
653 chemical measurements within the western Gulf of Mexico. Journal of Geophysical Research:
654 Oceans, 88(C4), 2601-2608. https://doi.org/10.1029/JC088iC04p02601, 1983.
655

Müller-Karger, F. E., McClain, C. R., Fisher, T. R., Esaias, W. E., and Varela, R.: Pigment distribution in the Caribbean Sea: Observations from space, Progress in Oceanography, 23(1), 23-64, https://doi.org/10.1016/0079-6611(89)90024-4, 1989.

Müller-Karger, F. E., Smith, J. P., Werner, S., Chen, R., Roffer, M., Liu, Y., Muhling, B., Lindo-Atichati, D., Lamkin, J., Cerdeira-Estrada, S., and Enfield, D.B.: Natural variability of surface oceanographic conditions in the offshore Gulf of Mexico, Progress in Oceanography 134:54-76, https://doi.org/10.1016/j.pocean.2014.12.007, 2015.

Müller-Karger, F. E., Walsh, J. J., Evans, R. H., and Meyers, M. B.: On the seasonal phytoplankton concentration and sea surface temperature cycles of the Gulf of Mexico as determined by satellites, Journal of Geophysical Research, 96(C7), 12645, https://doi.org/10.1029/91JC00787, 1991.

National Academies of Sciences, Engineering, and Medicine: Understanding and Predicting the Gulf of Mexico Loop Current: Critical Gaps and Recommendations, Washington, DC: The National Academies Press, https://doi.org/10.17226/24823, 2018.

Niiler, P. P.: Observations of low-frequency currents on the West Florida continental shelf, Memoires Societé Royale des Sciences de Liege, 6, 331-358, 1976.

Nof, D.: The momentum imbalance paradox revisited, Journal of Physical Oceanography, 35(10), 1928-1939, https://doi.org/10.1175/JPO2772.1, 2005.

Nowlin, W. D., and McLellan, H. J.: A characterization of Gulf of Mexico waters in winter, Journal

679 of Marine Research, 25(1), 29-59, 1967.
680
681 Oey, L.-Y.: Effects of winds and Caribbean eddies on the frequency of Loop Current eddy
682 shedding: A numerical model study, Journal of Geophysical Research, 108(C10), 1–25,
683 https://doi.org/10.1029/2002JC001698, 2003.
684
685 Oey, L.-Y., Ezer, T., Forristall, G., Cooper, C., DiMarco, S., and Fan, S.: An exercise in forecasting
686 loop current and eddy frontal positions in the Gulf of Mexico, Geophysical Research. Letters,
687 32(12), L12611, https://doi.org/10.1029/2005GL023253, 2005.
688
689 Paluszkiewicz, T., Atkinson, L. P., Posmentier, E. S., and McClain, C. R.: Observations of a Loop
690 Current frontal eddy intrusion onto the West Florida Shelf, Journal of Geophysical Research:
691 Oceans, 88(C14), 9639-9651, https://doi.org/10.1029/JC088iC14p09639,1983.
692
693 Pasqueron de Fommervault, O., Perez-Brunius, P., Damien, P., and Sheinbaum, J.: Temporal
694 variability of chlorophyll distribution in the Gulf of Mexico: bio-optical data from profiling floats,
695 Biogeosciences, 14, 5647-5662, https://doi.org/10.5194/bg-14-5647-2017, 2017.
696
697 Pichevin, T., and Nof, D.: The momentum imbalance paradox, Tellus, Series A: Dynamic
698 Meteorology Oceanography, 49(2), 298–319, https://doi.org/10.3402/tellusa.v49i2.14484, 1997.
699
700 Pichevin, T., Nof, D., and Lutjeharms, J.: Why are there Agulhas rings?, Journal of Physical
701 Oceanography, 29(4), 693-707, https://doi.org/10.1175/1520-

0485(1999)029<0693:WATAR>2.0.CO;2, 1999.

Polovina, J. J., Howell, E. A., and Abecassis, M.: Ocean's least productive waters are expanding, Geophysical Research Letters, 35(3), 2–6, https://doi.org/10.1029/2007GL031745, 2008.

Portela, E., Tenreiro, M., Pallàs-Sanz, E., Meunier, T., Ruiz-Angulo, A., Sosa-Gutiérrez, R., and Cusí, S.: Hydrography of the Central and Western Gulf of Mexico. Journal of Geophysical Research: Oceans, 123(8), 5134–5149. https://doi.org/10.1029/2018JC013813, 2018.

Richardson, P. L.: Eddy kinetic energy in the North Atlantic from surface drifters, Journal of Geophysical Research: Oceans, 88(C7), 4355-4367, https://doi.org/10.1029/JC088iC07p04355, 1983.

Savidge, D. K., and Bane, J. M.: Cyclogenesis in the deep ocean beneath the Gulf Stream. I-Description, Journal of Geophysical Research, 104, 18, https://doi.org/10.1029/1999JC900132, 1999.

Schmitz, W. J., Jr., Biggs, D. C., Lugo-Fernandez, A., Oey, L.-Y., and Sturges, W.: A synopsis of the circulation in the Gulf of Mexico and on its continental margins. In Circulation in the Gulf of Mexico: Observations and Models, Geophysical Monograph Series, 161, 11–30, https://doi.org/10.1029/161GM03, 2005.

Schmitz, W. J., Jr., and McCartney, M. S.: On the North Atlantic circulation, Reviews of Geophysics, 31(1), 29–50, https://doi.org/10.1029/92RG02583, 1993.

Sturges, W. and Lugo-Fernandez, A.: Circulation in the Gulf of Mexico: Observations and Models, Geophysical Monograph Series, 161, 347 pp. https://doi.org/10.1029/GM161, 2005

Sudre, J., Maes, C., and Garcon, V.: On the global estimates of geostrophic and Ekman surface currents, Limnology and Oceanography: Fluids and Environments, 3, 1–20, https://doi.org/10.1215/21573689-2071927, 2013.

Vukovich, F. M.: Loop Current boundary variations, Journal of Geophysical Research, Oceans, 93(C12), 15,585-15,591, https://doi.org/10.1029/JC093iC12p15585, 1988.

Vukovich, F. M., Crissman, B. W., Bushnell, M., and King, W. J.: Some aspects of the oceanography of the Gulf of Mexico using satellite and in situ data, Journal of Geophysical Research, 84, 7749, https://doi.org/10.1029/JC084iC12p07749, 1979.

Wei, M., Jacobs, G., Rowley, C., Barron, C. N., Hogan, P., Spence, P.,... & Coelho, E.: The performance of the US Navy's RELO ensemble, NCOM, HYCOM during the period of GLAD at-sea experiment in the Gulf of Mexico. Deep Sea Research Part II: Topical Studies in Oceanography, 129, 374-393, https://doi.org/10.1016/j.dsr2.2013.09.002, 2016.

Zavala-Hidalgo, J., Morey, S. L., and O'Brien, J. J.: Cyclonic Eddies Northeast of the Campeche Bank from Altimetry Data, Journal oh Physical Oceanography, 33(3), 623–629,

https://doi.org/10.1175/1520-0485(2003)033<0623:CENOTC>2.0.CO;2, 2003.

Zavala-Hidalgo, J., Morey, S. L., O'Brien, J. J., and Zamudio, L.: On the Loop Current eddy shedding variability, Atmosfera, 19(1), 41–48, 2006.

Zeng, X., Li, Y., and He, R.: Predictability of the loop current variation and eddy shedding process in the Gulf of Mexico using an artificial neural network approach, Journal of Atmospheric and Oceanic Technology, 32(5), 1098-1111, https://doi.org/10.1175/JTECH-D-14-00176.1, 2015.

Zharkov, V., and Nof, D.: Why Does the North Brazil Current Regularly Shed Rings but the Brazil Current Does Not?, Journal of Physical Oceanography, 40(2), 354-367, https://doi.org/10.1175/2009JPO4246.1, 2010.

Table 1. Average bold numbers for *Chl-a* concentrations (*mg m^{-3}*) and differences (*mg m^{-3}*; (%)) between Early and Contemporary averages at two geographical areas: 95.5˚W, 22.12˚N and 91.5˚W, 25.87˚N, (Western GoM) and 86˚W, 22.12˚N and 84.75˚W, 23.37˚N (LC-LCEs) during "**early**" (1998-2002), "**middle**" (2003-2008), and "**contemporary**" (2009-2014) epochs. Table 1 shows the compared averages in bold print. Standard deviations and number of pixels considered are shown in parenthesis.

Geographical Areas	Season	Early Averages (1998-2002)	Middle Averages (2003-2008)	Contemp. Averages (2009-2014)	Difference (Early-Contemp)
Western GoM	Winter	**0.180** (±0.047, n=4026)	**0.167** (±0.048, n=4866)	**0.173** (±0.0624, n=4828)	**0.007 (4%)**
Loop Current		**0.149** (±0.052, n=536)	**0.129** (±0.064, n=647)	**0.117** (±0.062, n=645)	**0.032 (21%)**
Western GoM	Spring	**0.114** (±0.033, n=3693)	**0.087** (±0.049, n=4658)	**0.0834** (±0.036, n=4754)	**0.030 (27%)**
Loop Current		**0.0948** (±0.074, n=526)	**0.085** (±0.1287, n=642)	**0.0835** (±0.116, n=648)	**0.011 (12%)**
Western GoM	Summer	**0.0887**(±0.024, n=3924)	**0.080** (±0.022, n=4794)	**0.0755** (±0.023, n=4837)	**0.013 (15%)**
Loop Current		**0.109** (±0.217, n=535)	**0.091** (±0.171, n=647)	**0.0938** (±0.148, n=648)	**0.015 (14%)**
Western GoM	Autumn	**0.151** (±0.052, n=3894)	**0.137** (±0.044, n=4876)	**0.127** (±0.043, n=4846)	**0.024 (16%)**
Loop Current		**0.138** (±0.128, n=525)	**0.1325** (±0.114, n=643)	**0.122** (±0.103, n=648)	**0.016 (12%)**

FIGURE CAPTIONS:

Fig. 1. Monthly means of absolute dynamic topography (ADT) and surface currents averaged over a quarter of a century (1993-2017).

Fig. 2. Climatological monthly maps of eddy kinetic energy (EKE) in GoM: red color contours correspond to the areas of maxima EKE. The heavy black line corresponds to the isoline of 40 *cm* 2.2 *cm* of the CWF (the contour of the CWF is significant at the 95% of level). The EKE was calculated using daily maps of satellite-derived currents from AVISO (GEKCO) for a quarter of a century (1993 – 2017).

Fig. 3. Geographical positions of the CWF tracked using the 40 *cm* ADT isoline representing 1993-2017 monthly average values: a) Northward and b) Westward, respectively; c) ADT spectral analysis in a region influenced by the CWF (91.25ºW, 23.125ºN and 83.5ºW, 28.12ºN).

Fig. 4. The ADT quarter-century CWF (1993-2017) monthly climatology and its standard deviation are shown in heavy and dotted lines, respectively. The heavy line corresponds to the 40 *cm* isoline of the CWF. The dotted line encloses values of the standard deviation >15 *cm*.

Fig. 5. Average monthly percentage surface areas of CW in the interior of the Gulf of Mexico determined from climatology of the STD contour > 15 *cm*; enclosed areas were calculated in relation to the GoM area (1.56×10^6 km^2).

Fig. 6. Monthly means of absolute dynamic topography (ADT) from 1993-2002 (color) and its respective CWF computed with the 40 *cm* isoline (heavy black line).

Fig. 7. Monthly means of absolute dynamic topography (ADT) from 2003-2017 (color) and respective CWF computed with the 40 *cm* isoline (heavy black line).

Fig. 8. Monthly climatologies of *Chl-a* (SeaWIFS, 1998-2002 and MODIS data source, 2003-2017). The heavy black line represents the contour of the 40 *cm* ADT data that represents the CWF (1998-2017). *Chl-a* values larger than 1 $mg\ m^{-3}$ are plotted in red.

Fig. 9. From top left to bottom right, average *Chl-a* values according to period: column 1, SeaWIFS 1998-2002, column 2, MODIS 2003-2008, and column 3, MODIS 2009-2014. From top to bottom figures correspond to the mean seasons. Average *Chl-a* concentration is computed inside the white and red squares (white corresponds to the western GoM and red corresponds to the LC area). Average values for each time period and season are in Table 1.

Fig. 10. Differences of *Chl-a* concentration ($mg\ m^{-3}$) between 2009-2014 average values of MODIS data minus 1998-2002 average SeaWIFS values. The broken line represents the 250 *m* isobath. White contoured areas indicate no significant differences.

Fig. 11. *Chl-a* concentrations ($mg\ m^{-3}$) at four stations (a to d) in the GoM, daily time series derived from SeaWIFS from 1998 to 2002 (green) and MODIS from 2003 to 2017 (blue). Least square regressions for SeaWIFS (red line), MODIS (cyan line), and the overall linear regressions for each station (dashed black line).

815 FIGURE 1

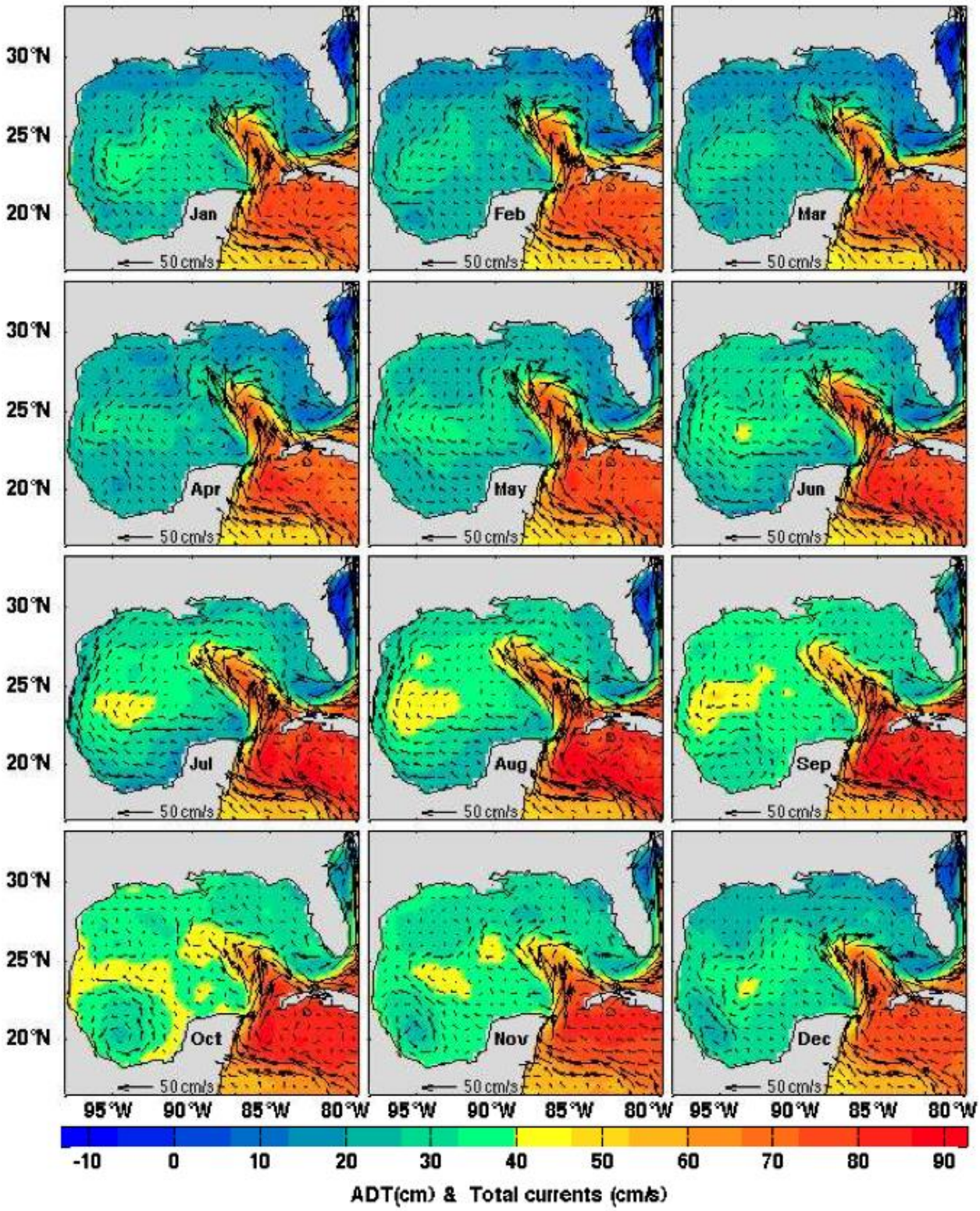

816

817

818 FIGURE 2

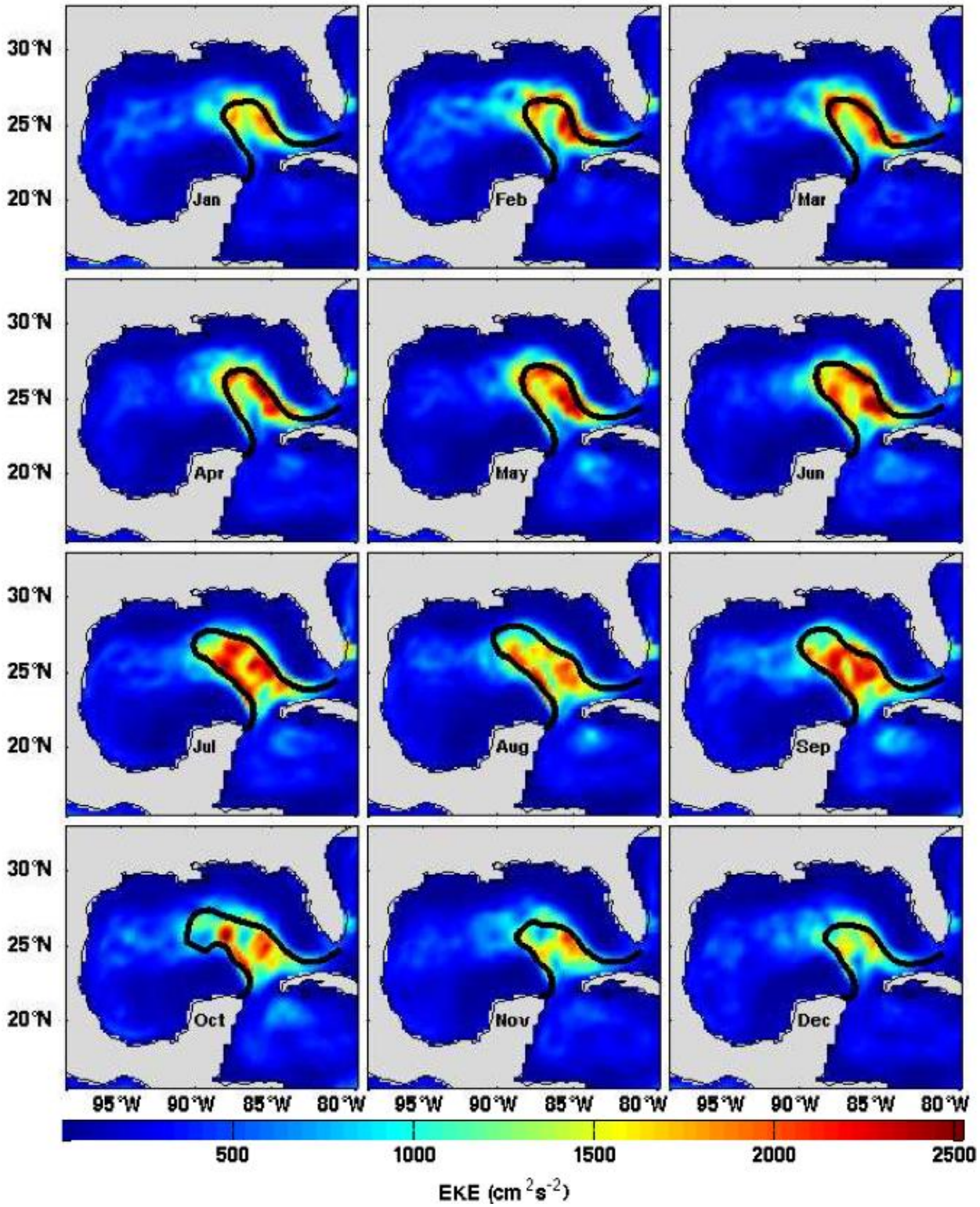

819

820

821 FIGURE 3

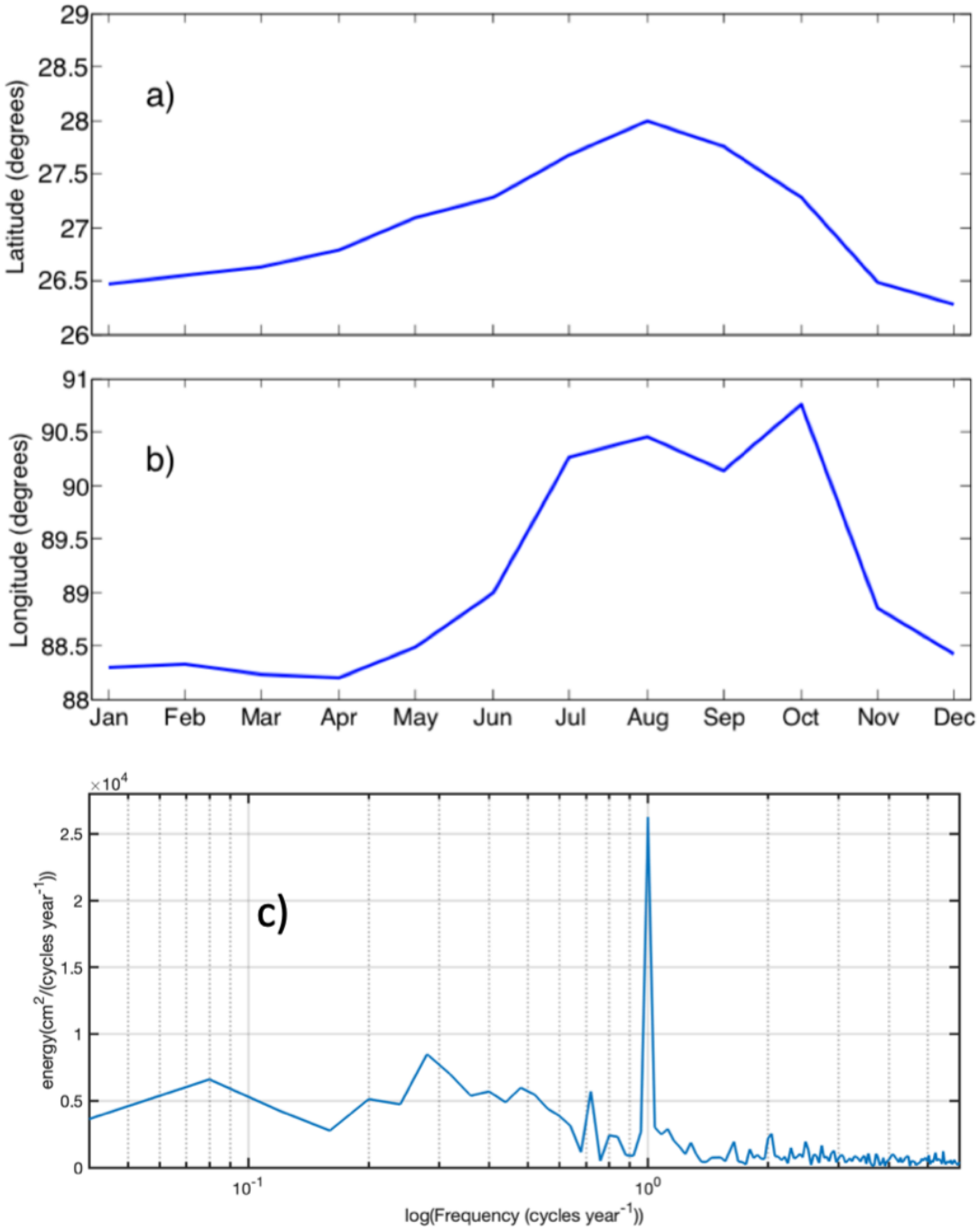

822

823

824

825 FIGURE 4

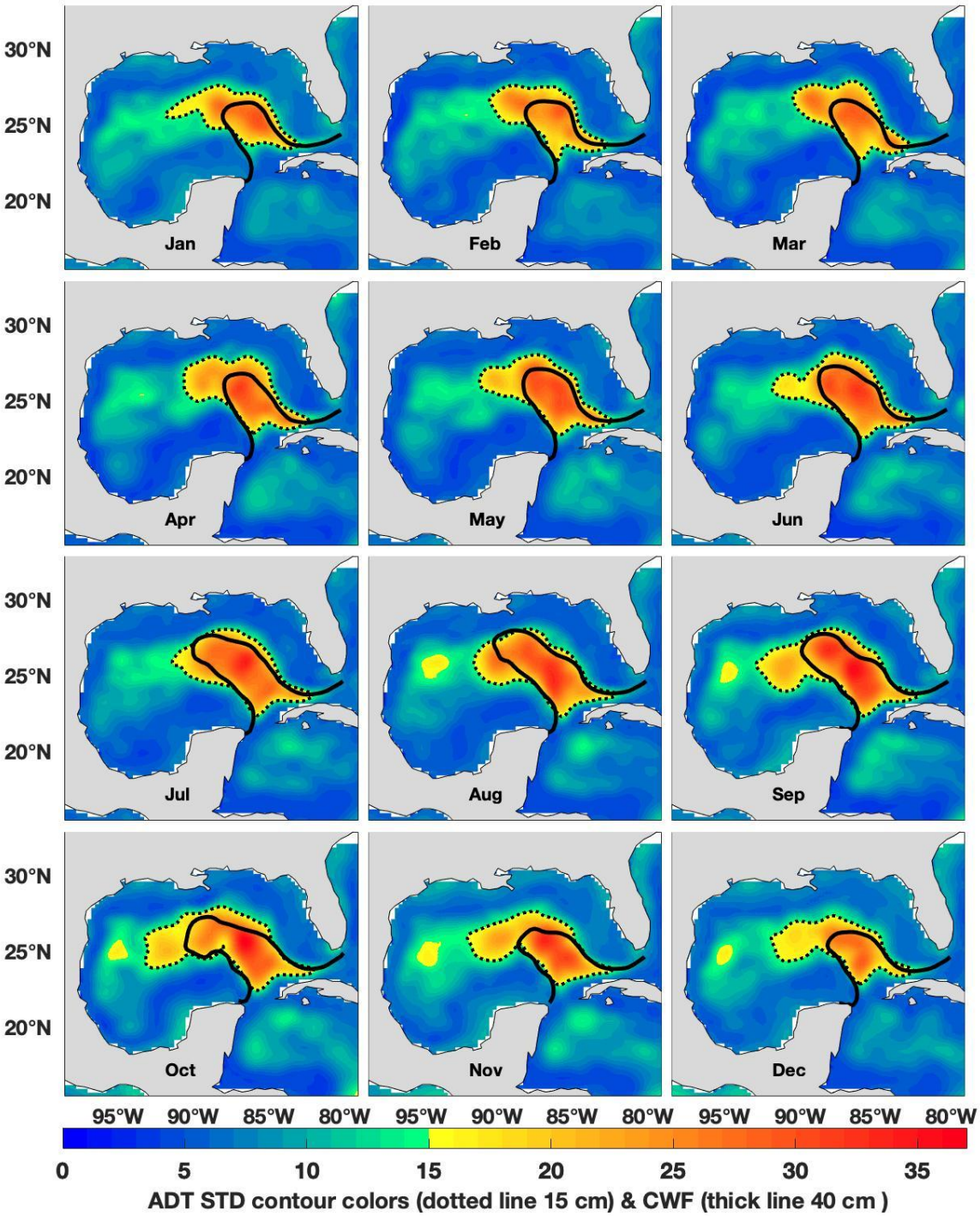

826

827

828

829 FIGURE 5

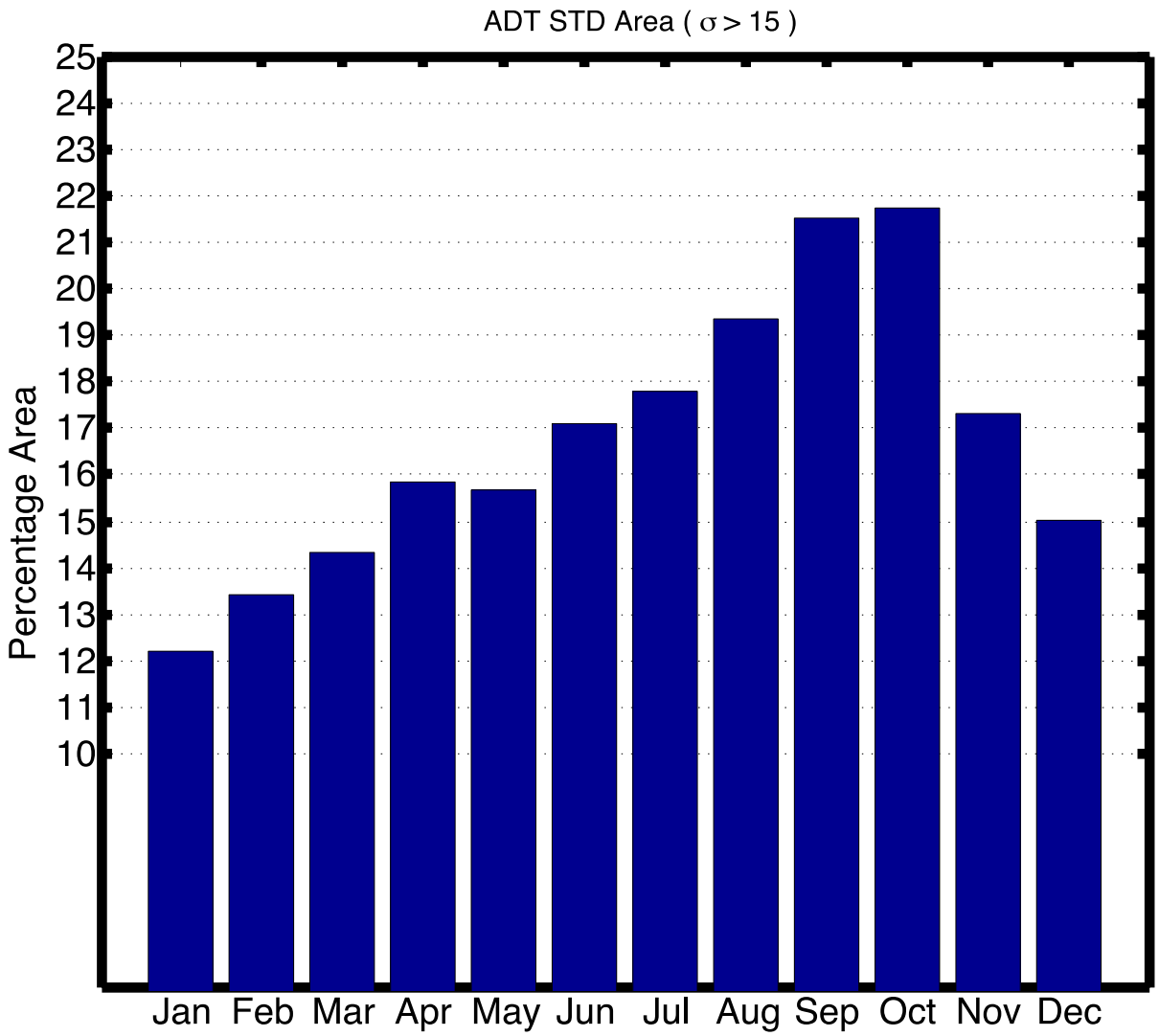

830

831

832

833

834

835

836

837

838 FIGURE 6

839

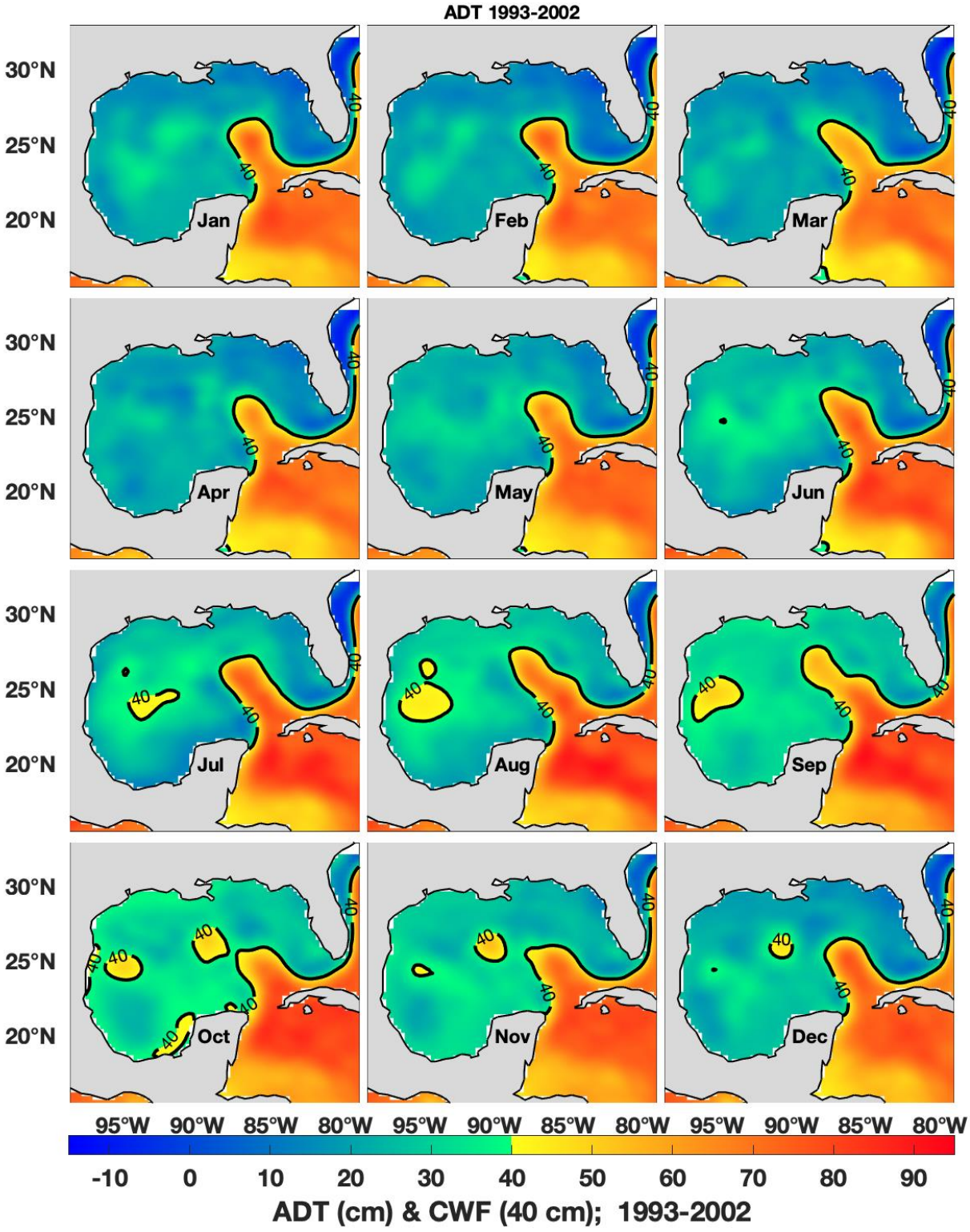

840

841 FIGURE 7

842

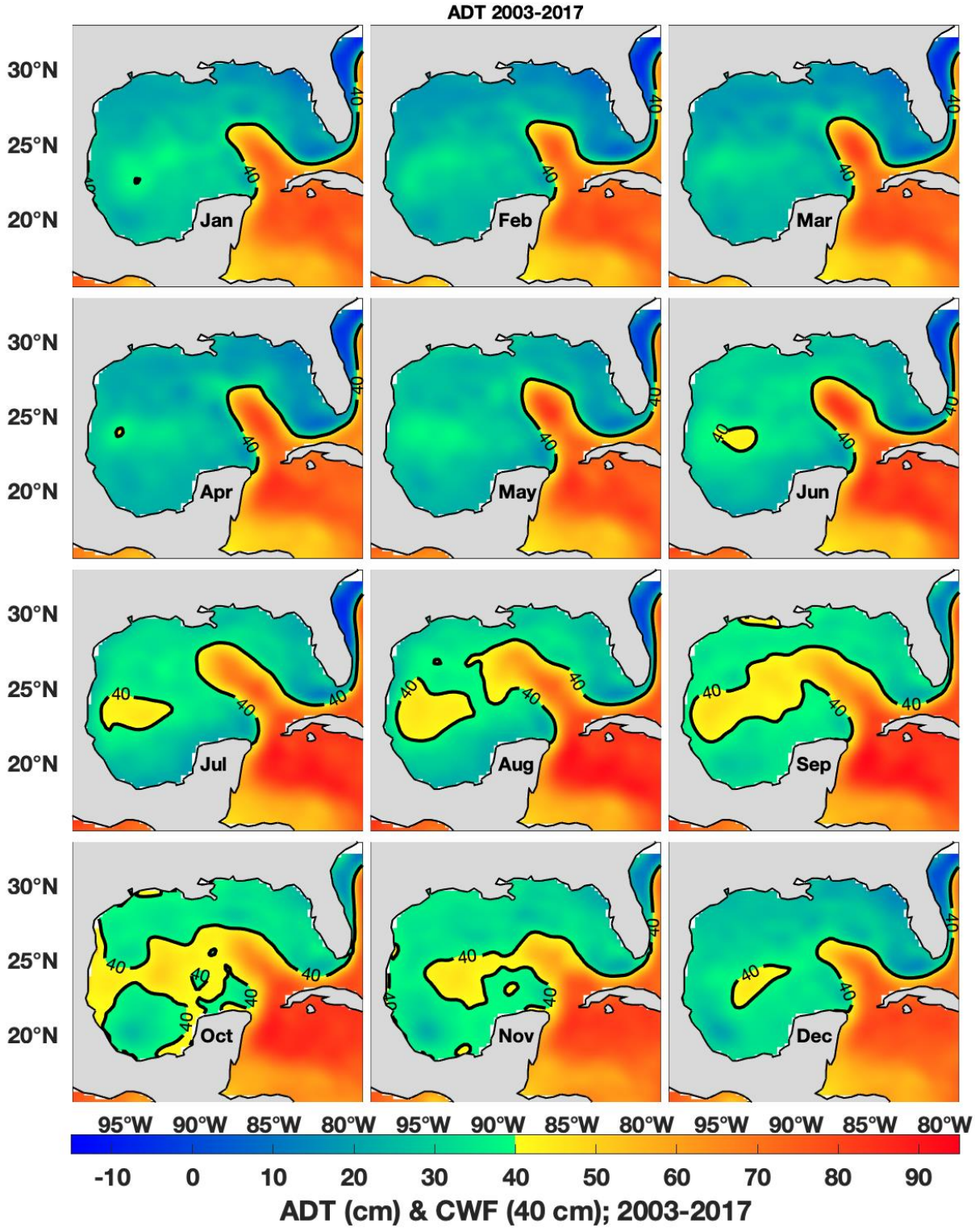

843

844 FIGURE 8

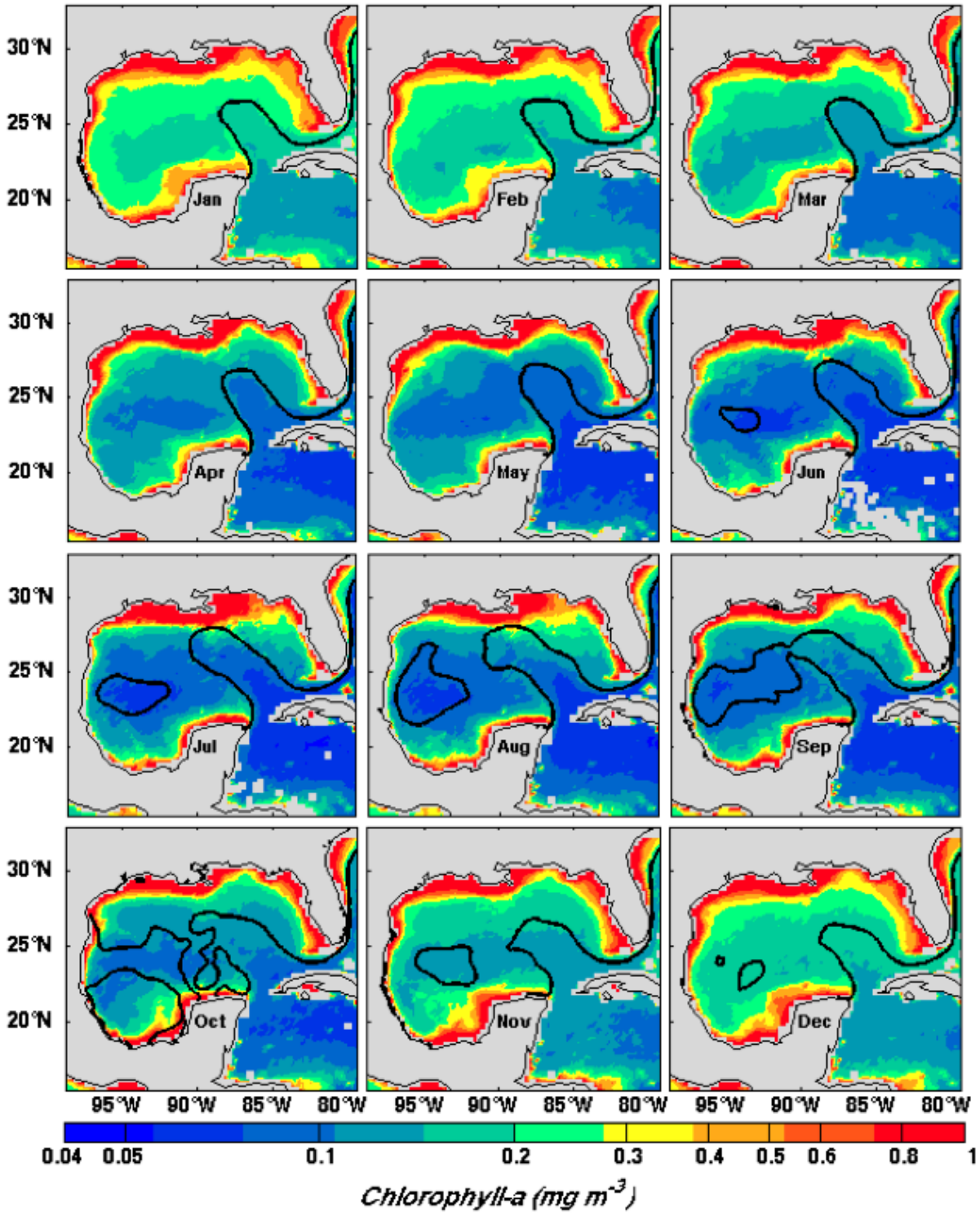

845

846

847 FIGURE 9

848

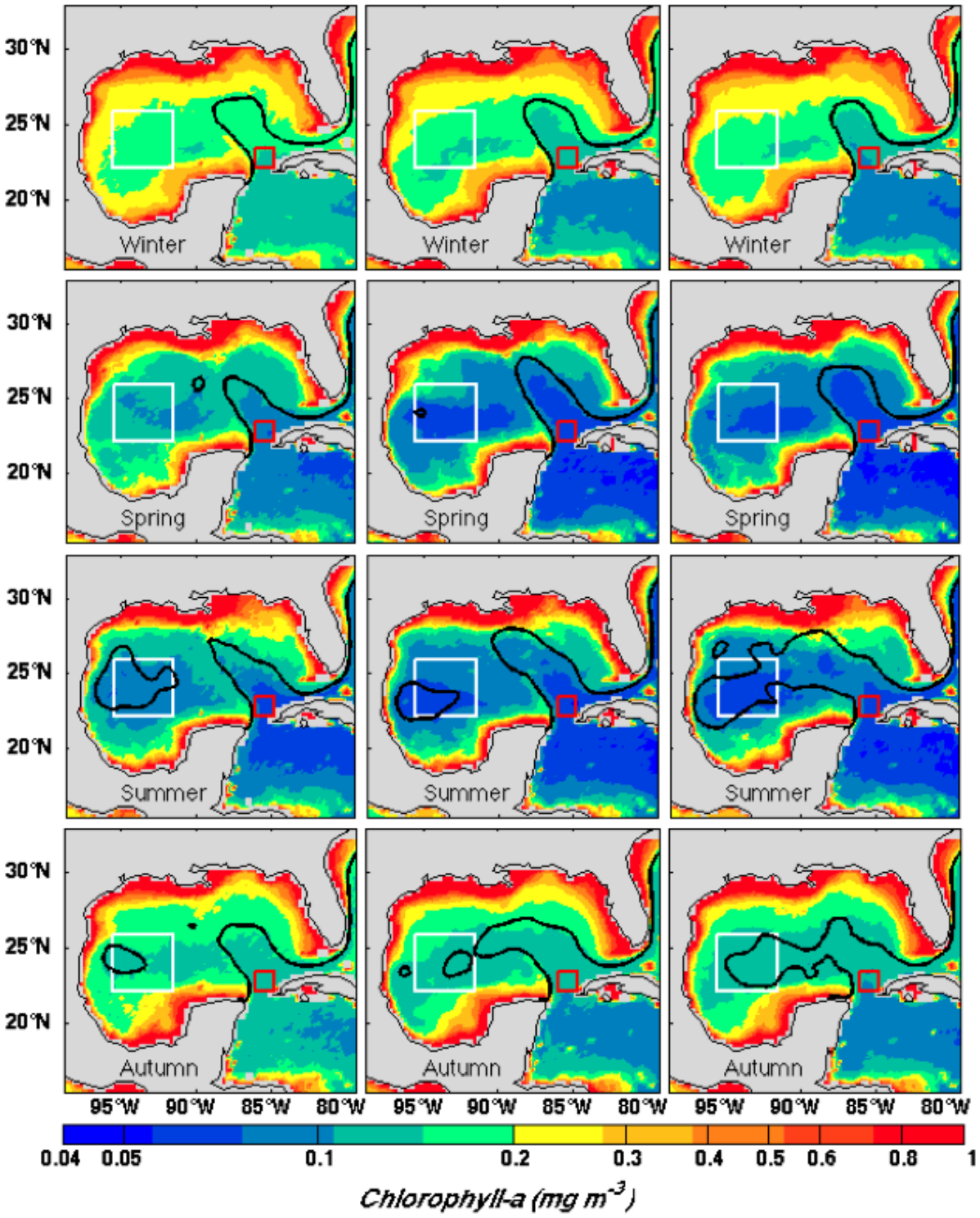

849

850

851 FIGURE 10

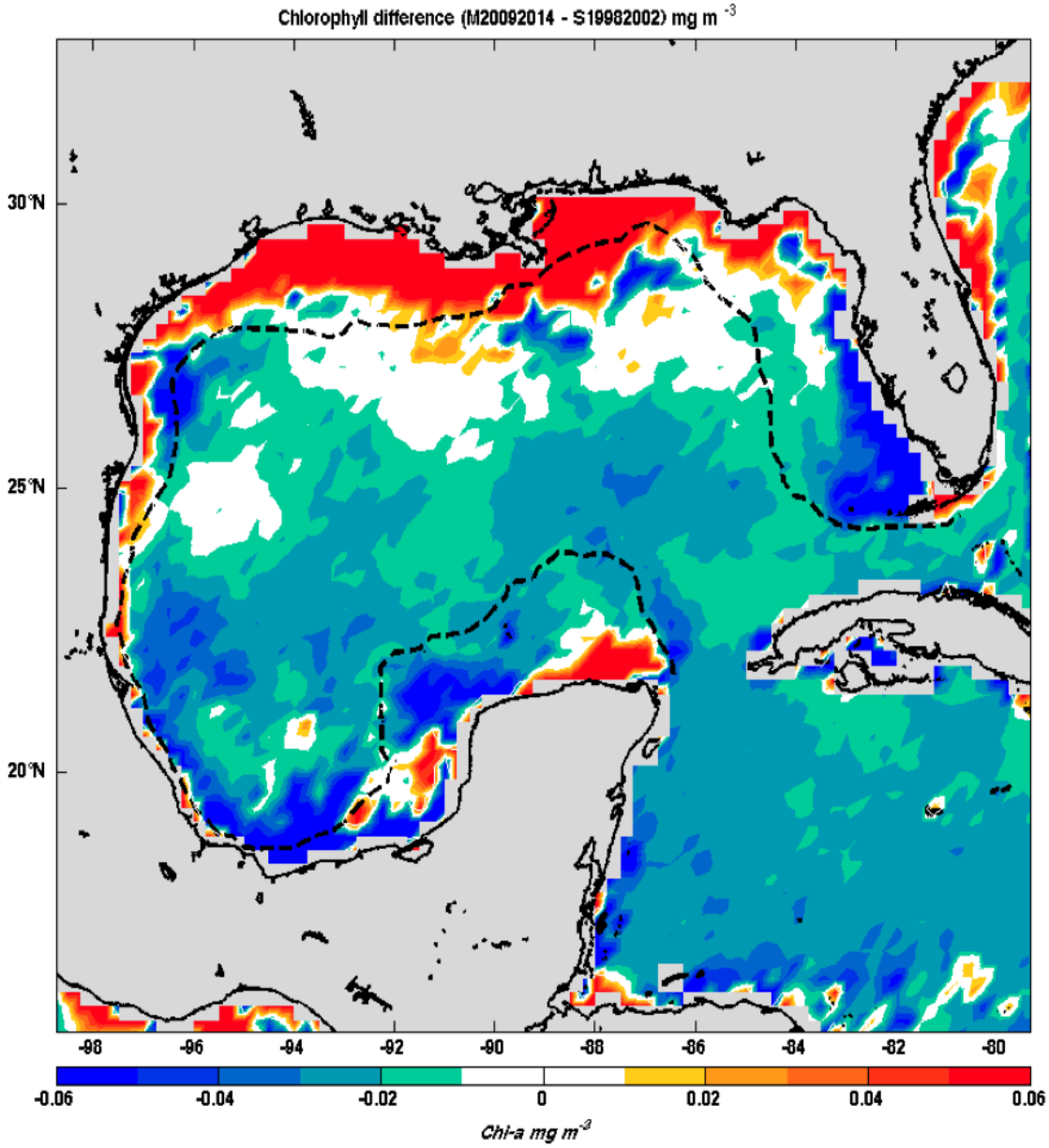

852

853

854

855

856

857

858

859 FIGURE 11

860

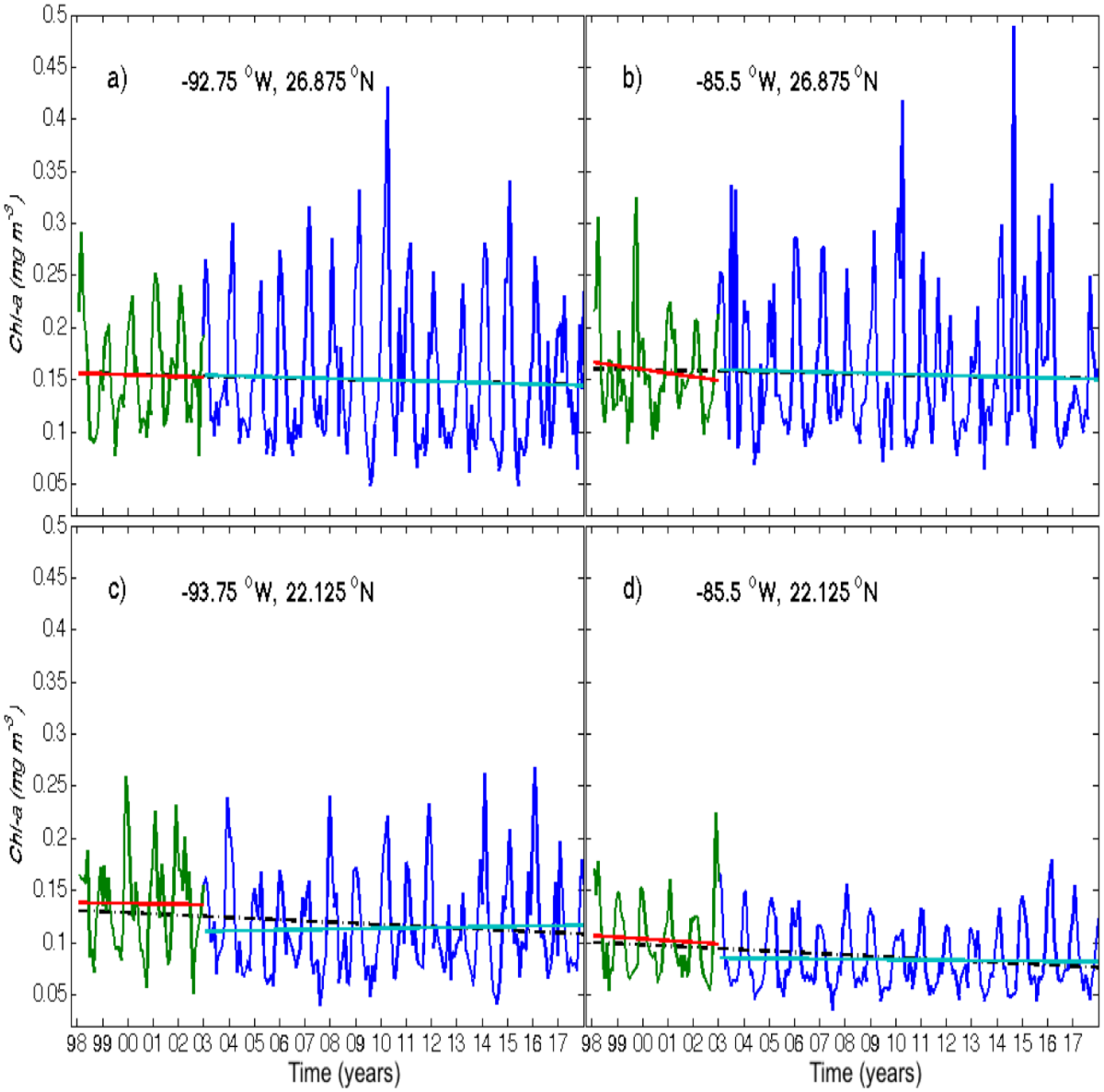

861

862

863

864